The DNA Damage Checkpoint Protein ATM Promotes Hepatocellular Apoptosis and Fibrosis in a Mouse Model of Non-Alcoholic Fatty Liver Disease

A Thesis

Presented to the Faculty of the Graduate School

of Cornell University

in Partial Fulfillment of the Requirements for the Degree of

Master of Science

by

Erin Daugherity, D.V.M.

January, 2013

ABSTRACT

Steatoapoptosis is a hallmark of non-alcoholic fatty liver disease (NAFLD) and is an important factor in liver disease progression. We hypothesized that increased reactive oxygen species resulting from excess dietary fat contribute to liver disease by causing DNA damage and apoptotic cell death, and tested this by investigating the effects of feeding mice a high fat or standard diets for 8 weeks. High fat diet feeding resulted in increased hepatic H_2O_2, superoxide production, and expression of oxidative stress response genes, confirming that the high fat diet induced hepatic oxidative stress. High fat diet feeding also increased hepatic steatosis, hepatitis, and DNA damage as exemplified by an increase in the percentage of 8-hydroxyguanosine (8-OHG) positive hepatocytes in high fat diet fed mice. Consistent with reports that the DNA damage checkpoint kinase Ataxia Telangiectasia Mutated (ATM) is activated by oxidative stress, ATM phosphorylation was induced in the livers of wild-type mice following high fat diet feeding. We therefore examined the effects of high fat diet feeding in *Atm*-deficient mice. The prevalence of apoptosis and expression of the pro-apoptotic factor Puma were significantly reduced in *Atm*-deficient mice fed the high fat diet when compared to wild-type controls. Furthermore, high fat diet fed $Atm^{-/-}$ mice had significantly less hepatic fibrosis than $Atm^{+/+}$ or $Atm^{+/-}$ mice fed the same diet. Together, these data demonstrate a prominent role for the ATM pathway in the response to hepatic fat accumulation and link ATM activation to fatty liver-induced steatoapoptosis and fibrosis, key features of NAFLD progression.

BIOGRAPHICAL SKETCH

Erin Daugherity was born in Ithaca, New York. She received a Bachelor of Science in 2001 from Cornell University following completion of the Animal Sciences major. She received a Doctorate of Veterinary Medicine from University of Wisconsin-Madison in 2007. Following veterinary school, she completed a Laboratory Animal Medicine Residency at Cornell University within the Cornell Center for Animal Resources and Education, as well as a Clinical Fellowship within the department of Biomedical Sciences. During the residency she was accepted into the Cornell Graduate School in the Field of Comparative Biomedical Sciences from which she will be receiving a Master of Science in August 2012.

This is dedicated to my family for continued and endless love and support.

ACKNOWLEDGMENTS

I would like to thank Bob Weiss and Kirk Maurer for excellent support, mentorship, laboratory support and guidance throughout this project. These two individuals had a major impact on my career path and I am very lucky to have them as mentors. Thank you to everyone in the Weiss lab. Without your help with protocols, bench work and ideas, this project would not have been possible. In particular, thank you to Gabi Balmus, Elizabeth Moore, and Ahmed Al Saei for help with various aspects of the project; and thank you to Amy Lyndaker, Pei Xin Lim, Minxing Li, Kelly Hume, Claire Anderson and Jack Stupinsky for endless support. I would like to thank the members of the Denkers' lab for project ideas and the use of substrates, especially Delbert Abi Abdallah for help with flow cytometry and confocal microscopy. I would also like to thank Arlin Rogers for help with special stains and pathological scoring. I would like to thank the department of Biomedical Sciences for departmental support and my co-workers and life-long friends in the Center for Animal Resources and Education (CARE) for support and the excellent care of animal used in teaching and research. Finally, I would like to thank Luce Guanzini for reading and editing this thesis and Drew Kirby for technical support.

TABLE OF CONTENTS

Note: The contents of this thesis were published in part in the manuscript, "Daugherity, E.K., Balmus, G., Al Saei, A., Moore, E.S., Abi Abdallah, D., Rogers, A.B., Weiss, R.S., and Maurer, K.J. (2012). The DNA damage checkpoint protein ATM promotes hepatocellular apoptosis and fibrosis in a mouse model of non-alcoholic fatty liver disease. Cell Cycle 11:1918-1928.

LIST OF FIGURES

LIST OF TABLES

CHAPTER ONE:

INTRODUCTION

The spectrum of Non-Alcoholic Fatty Liver Disease

Nonalcoholic fatty liver disease (NAFLD) is an emerging health epidemic with a poorly understood pathogenesis and limited therapeutic options [1]. Based on epidemiological, clinical and biochemical data, NAFLD is the hepatic manifestation of metabolic syndrome, which includes obesity, dyslipidemia, and insulin resistance [2]. NAFLD comprises a spectrum of hepatic lesions ranging from steatosis with deposition of triglycerides within hepatocytes to the more aggressive nonalcoholic steatohepatitis (NASH) which includes hepatitis and fibrosis [1,3]. Fatty liver disease is currently the most common chronic liver condition in Western countries and is highly prevalent in the U.S. with an estimated 30% of the population possessing NAFLD and 6% suffering from NASH (Figure 1). These numbers rise to 90% and 30% respectively when obese populations are examined [4]. Simple steatosis is generally considered to be benign, but

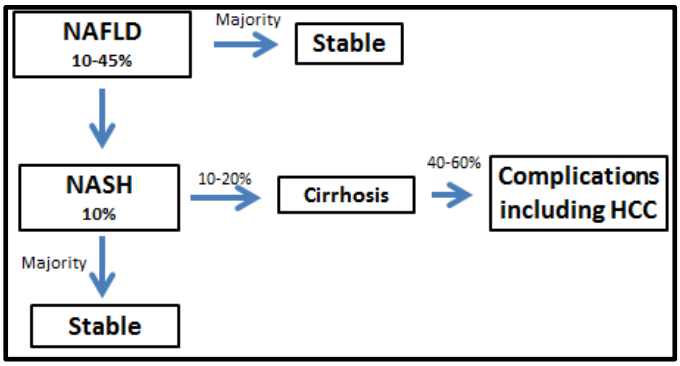

Figure 1: Prevalence of Non-alcoholic fatty liver disease. NAFLD describes a wide spectrum of liver disease, including hepatic cirrhosis and associated complications.

the accumulation of hepatic inflammatory infiltrates during NASH is considered to be the precursor to more aggressive liver disease. NASH-induced complications are severe and approximately one-third of NASH patients develop cryptogenic or idiopathic cirrhosis and may progress to hepatocellular carcinoma (HCC) [1,3,5].

Hepatocellular carcinoma (HCC)

Hepatocellular carcinoma is the most common primary cancer of the liver. It is currently the fifth most common cause of cancer worldwide, is the third leading cause of cancer death behind cancers of the lung and stomach and is increasing in incidence, particularly in industrialized countries [3,6]. Over the past 20 years in the United States, there has been an 80% increase in the yearly incidence of HCC despite a decrease in historical risk factors, which include chronic hepatitis B and C infection, alcohol consumption, aflatoxin exposure, and autoimmune hepatitis [3,6] . The major risk factor for the development of HCC is hepatic cirrhosis with cirrhosis being present in approximately 80%-90% of HCC patients, but approximately one fourth of HCC cases diagnosed in the United States do not possess known predisposing risk factors for cirrhosis [6,7]. Moreover, the increase in incidence of HCC over the past 20 years is thought to be due, in part, to the emergence of the spectrum of non-alcoholic fatty liver diseases, including cirrhosis formation in the liver. There is a clear link between dietary fat consumption, fatty liver disease, and hepatocellular carcinoma formation; however, the factors that promote the progression of NAFLD to NASH and its associated complications currently are not well understood [3,6,8,9].

Fatty liver disease and oxidative stress

The initial accumulation of lipids in the liver is considered the "first hit" during NAFLD pathogenesis and renders hepatocytes more susceptible to oxidative stress. Reactive oxygen species (ROS), including superoxide anion and hydrogen peroxide, are by-products of normal cellular metabolism. However, when excess amounts of substrate, such free fatty acids, are metabolized, harmful ROS accumulate within the cellular compartment [10]. Increase ROS production due to excess FFA has been demonstrated by numerous models of fatty liver disease [11,12]. Oxidative stress is a state where the generation of ROS exceeds the removal or redox of these products from the cell [10,13]. The presence of hepatic oxidative stress is regarded as the "second hit" of NAFLD pathogenesis. After inflammation accompanies the steatosis and the condition is considered NASH, there is an increase in oxidative stress, as well as the accumulation of fibrosis, more extensive liver damage, and in some cases, there is development of HCC [10,13,14,15]. Xu *et al* [16] revealed that hepatocytes deficient in nuclear respiratory factor 1 (Nrf1), a transcription factor which upregulates key antioxidant genes essential during oxidative stress, had increased susceptibility to oxidative stress which resulted in hepatic apoptosis, inflammation and fibrosis, and ultimately led to HCC development. Additionally, activation of inflammatory cell infiltrates contributes to reactive oxygen species (ROS) production and to the progression of NAFLD to NASH [17]. Overall, the occurrence of oxidative stress is a hallmark of fatty liver disease progression. In fact, it has been documented that higher levels of oxidative stress correlates with increasing disease severity.

Fatty liver disease, steatoapoptosis and carcinogenesis

During NAFLD/NASH, an excessive amount of nonesterified free fatty acids (FFAs) overwhelm the ability of the liver to convert FFAs to triglycerides, resulting in apoptotic cell death, a process known as steato- or lipo-apoptosis [18,19]. In both humans and animal models, hepatocyte apoptosis correlates with NASH severity and fibrosis stage, suggesting steatoapoptosis plays a causative role in disease progression[12,19,20,21,22]. However, the exact mechanisms and cellular pathways linking hepatic lipid accumulation to steatoapoptosis and the progression of NAFLD/NASH remain largely unknown. Oxidative stress may have a central role, as oxidative metabolism is increased in NAFLD patients [23] and recent studies indicate that saturated FFAs induce apoptosis through the generation of reactive oxygen species [22]. Excessive ROS production induces apoptosis via various pathways, including the extrinsic pathway of apoptosis which utilizes death receptor signaling, and the intrinsic pathway of apoptosis which involves mitochondrial and endoplasmic reticulum stress and p53 upregulated modulator of apoptosis (PUMA) signaling [20,24]. PUMA is a pro-apoptotic BH3-only protein that both directly and indirectly activates other members of the Bcl-2 protein family, such as Bax and Bak, ultimately leading to mitochondrial dysfunction and apoptosis [24,25].

In addition to the hypothesis that apoptosis provides a protective function against tumorigenesis, it has been hypothesized that apoptosis evasion contributes to early tumorigenesis in general, as well as resistance to chemotherapy [24]. Several recent studies utilizing PUMA-deficient mice revealed that loss of PUMA prevented γ-irradiation induced apoptosis, compensatory hematopoietic stem cell proliferation, and lymphomagenesis, suggesting that cell death as well as progenitor cell expansion are needed for DNA damage induced tumor formation and that following apoptosis the repopulation with hepatic progenitor cells carrying mutations

can drive tumorigenesis [24,26,27]. Moreover, Luedde et al [28] revealed that inhibiting hepatic NF-κB, an anti-apoptotic inflammatory cytokine that is activated in many tumor types, resulted in steatohepatitis, increased apoptosis, and HCC development, most likely through compensatory hepatic proliferation. Interestingly, this phenomenon is also seen in patients with viral or alcohol induced HCC where hepatocytes and bi-potential oval cells serving as functional stem cells of the liver repeatedly proliferate through cycles of hepatocyte death and regeneration [29,30]. Additionally, chemotherapy failure can be caused by re-population with drug resistant stem cells [30,31]. Conversely, mouse models indicate that PUMA deficiency accelerates c-Myc induced lymphomagenesis and chemical induced intestinal tumorigenesis [24,32,33]. In addition, Nakanishi et al [34] established that runt-related transcription factor 3 (RUNX3), a pro-apoptotic factor and gastric cancer tumor suppressor that is downregulated in 30-80% of HCCs, increases starvation-induced apoptosis in HCC cell lines and that deleting RUNX3 leads to tumorigenesis by escaping apoptosis. Collectively, these studies suggest that either an increase or decrease in apoptosis can have both a causal and a protective effect on hepatic carcinogenesis.

Fatty liver disease, hepatic fibrosis and carcinogenesis:

It is well established that chronic liver injury, as seen during fatty liver disease progression, results in progressive fibrinogenesis caused predominantly by the activation of hepatic stellate cells to a myofibroblast phenotype thereby producing excess extracellular matrix. Importantly, advanced fibrosis is the largest single risk factor for HCC development [6,35,36,37]. This risk is emphasized in a current case study from Japan of patients with

diagnosed NASH that progressed to HCC where cirrhosis was present in 51% of the cases and advanced stages of fibrosis were present in 72% of the cases [37].

Significant pro-fibrinogenic mechanisms include oxidative stress and chronic inflammation. A recent model proposed by Matsuzaki identifies chronic inflammation as a predominant fibro-carcinogenesis driver via Smad protein signaling, which conveys signals from TGF-β receptors to the nucleus, including a shift from the pSmad3C to the pSmad3L pathway thus accelerating liver fibrosis and increasing the risk of HCC[35]. Therefore, hepatic fibrotic and inflammatory responses provide a link between fatty liver disease hepatocarcinogenesis.

Fatty liver disease, DNA damage and HCC formation:

The exact mechanism of carcinogenesis during NAFLD/NASH remains unknown, but three essential components of carcinogenesis are thought to be involved, including carcinogenesis initiation due to oxidative stress and lipid peroxidation; carcinogenesis promotion due to hepatocellular apoptosis and proliferation; and neoplastic progression due to oxidation-induced mutations [3,6]. ROS can induce DNA damage and is one of the most common causes of hepatic genomic instability [38]. Oxidized bases are repaired primarily by the DNA base excision repair (BER) pathway. 8-Hydroxyguanosine (8-OHG), an oxidized form of the nucleotide guanine, is the major product produced when DNA is oxidatively attacked. If left un-repaired, 8-OHG results in A:T to C:G or G:C to T:A transversion mutations in both mitochondrial and nuclear nucleic acids and causes genomic instability [10,13]. It is clear that oxidative stress and DNA damage play a role during the progression of fatty liver disease to hepatic carcinogenesis; thus, utilizing a model that is involved in both DNA damage and repair

and the cellular response to ROS accumulation is essential to determining the exact links between hepatic fat accumulation and hepatocellular carcinoma formation.

Ataxia Telangiectasia and the Ataxia Telangiecatsia Mutated (ATM) protein kinase

Ataxia-Telangiectasia (A-T) is a rare autosomal recessive disorder in humans caused by the deficiency of the protein kinase ataxia telangiectasia mutated (ATM). Worldwide, there is one case of A-T in every 40,000 to 100,000 live births [39]. The majority of A-T patients generate non-functional, unstable, truncated ATM protein due to missense or nonsense mutations in the *ATM* gene [40]. ATM is a member of the phosphoinositide 3-kinase-related protein kinase (PIKK) family of Ser/Thr-protein kinases, which also includes ataxia-telangiectasia and RAD-3related (ATR), DNA-dependent protein kinase catalytic subunit (DNA-PKcs) and mammalian target of rapamycin (mTOR) [41,42]. ATM is a major cellular regulator of the response to double strand DNA breaks (DSB), and consequently, A-T patients cannot respond to DSB properly, resulting in a variety of deleterious phenotypes including progressive cerebellar ataxia, oculocutaneous telangiectasia, immunodeficiency, premature aging, sterility, chromosomal instability, shortened lifespan, sensitivity to ionizing radiation and cancer predisposition, particularly lymphoid tumorigenesis [41,43]. Moreover, polymorphisms and mutations in the *Atm* gene are linked to an elevated cancer risk, including lung and breast cancer, glioma, and hereditary pancreatic ductal adenocarcinoma [44,45,46]. Further, immune system phenotypes are most likely due to the inability to process and repair DNA strand breaks that naturally occur during V(D)J and class switch recombination [47,48].

ATM and the DNA damage response

Members of the PIKK family protect the genomic integrity of eukaryotic cells through the activation of cell cycle checkpoints and by activating DNA repair. While ATR is activated by single stranded DNA, both ATM and DNA-PKcs are activated by DNA DSBs but initiate different DNA repair pathways. DNA-PKcs is recruited and activated by the interaction with Ku heterodimer and promotes the non-homologous enjoining DNA repair pathway. Conversely, ATM is activated by DNA damage through interactions with the MRE-11-RAD50-NBS1 (MRN) complex and promotes DNA repair through the homologous recombination pathway following DNA end-processing [41]. Failure to activate ATM after DNA damage leads to defective cell cycle control and impaired DNA repair.

ATM exists as an inactive dimer that undergoes autophosphorylation at Ser1981and subsequent monomerization during activation due to DNA damage [49]. Autophosphorylation of ATM at Ser1981 is required for the retention of ATM at the site of the DSB, but is not required for the recruitment of ATM to the site of damage [50]. Once activated, ATM regulates the G_1-S cell cycle checkpoint through phosphorylation of p53 at Ser15 and checkpoint kinase 2 (CHK2) at Thr68 [51,52], which then phosphorylates intermediary protein substrates including BRCA1, CDC25A , and CDC25 [41]. Additionally, phosphorylation of the histone H2AX, a marker of DNA double stranded breaks, occurs concurrently with ATM activation due to DNA damage [42]. ATM also regulates the intra-S checkpoint through the phosphorylation of SMC1 [42]. Furthermore, ATM-induced p53 phosphorylation leads apoptosis and senescence if the DNA damage cannot be properly repaired (Figure 2) [51,53]. Finally, several hundred ATM substrates have been identified following ionizing radiation, which induces DNADSBs, many of which have roles in the DNA damage response or function during cell cycle checkpoint arrest, but also

include targets that dot not play a role in these pathways [54]. Additionally, there are numerous phosphorylation events that occur as a result of DNA damage that are ATM-dependent but are not directly catalyzed by ATM, further highlighting the central role ATM plays in the cellular response to DNA damage.

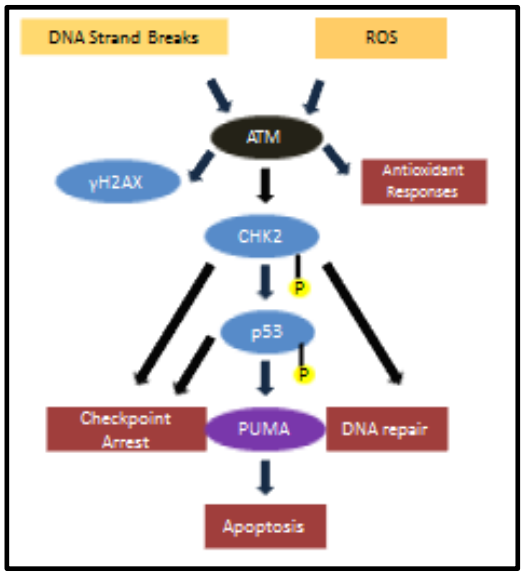

Figure 2: The ATM pathway is activated due to DNA double stranded breaks and directly by ROS. ATM activation either by double strand breaks or by ROS results in the activation of many downstream, substrates, including CHK2 and p53, which then activates pro-apoptotic PUMA, leading to cell cycle checkpoint arrest and DNA repair, or to apoptosis. When activated by double strand breaks, there is concurrently phosphorylation of H2AX, which is not seen when ATM is directly activated by ROS.

ATM and the cellular response to oxidative stress

Various studies suggest that the neurodegenerative phenotypes observed in A-T patients are not related to genomic instability caused by deficiency of ATM, but are the result of loss of ATM function independent of DNA damage, partly due to the fact that post-mitotic cerebellar

neurons do not completely rely on ATM-mediated cell cycle regulation [41]. Further, ATM is implicated in metabolic disease characterized by a variety of conditions including insulin resistance, glucose intolerance, elevated serum cholesterol and lipid levels, and atherosclerosis [41,55]. Evidence now links ATM deficiency with elevated oxidative stress and deregulation of cellular metabolic functions. For instance, ATM deficient cells have reduced levels of antioxidant compounds and are hypersensitive to treatment with oxidizing agents, and this oxidative stress can be alleviated with the administration of antioxidant compounds [41,42]. Cultured *Atm*-deficient cells are more sensitive to oxidative stress [13] and hepatocytes with excess fat are exceptionally vulnerable to oxidative stress and DNA damage [5,10,23]. Moreover, a fraction of the ATM protein has been shown to be present in the cytoplasm of various cell types, notably in cerebellar neurons, despite the fact that it is considered to be generally localized to the nucleus [41]. These facts provide evidence for the role of ATM in cellular response to oxidative stress.

It is now known that ATM can be directly activated by ROS (Figure 2). When activated by ROS, ATM exists as an active dimer with two monomers covalently linked by disulfide bonds [41]. Guo *et al* [42] treated primary human fibroblasts with the oxidizing agent hydrogen peroxide (H_2O_2), or with bleomycin, which induces DNA DSBs. ATM autophosphorylation occurred in response to both treatments, and activation of ATM by H_2O_2 occurred independently of free DNA ends and the MRN complex. However, when the group mutated Serine 1981 to alanine in order to prevent ATM autophosphorylation, oxidized ATM retained the ability to phosphorylate downstream p53, demonstrating that autophosphorylation is not required for ATM activation by ROS [42]. Additional evidence supporting the hypothesis that ATM activation by ROS is a distinct mechanism from that during ATM activation by DNA damage, treatment of human fibroblasts with H_2O_2 resulted in subsequent phosphorylation of p53 and CHK2, but not

in phosphorylation of histone H2AX or the heterochromatin protein KAP1, both of which accompany DSB formation. This study also demonstrated that substrate specificity during ATM activation by ROS is not the same as the specificity during activation by DNA damage. Further, chromosomal abnormalities and oxidative DNA lesions in ATM null embryonic stem cells were also prevented with antioxidant treatment [56]. Li *et al* [57] demonstrated that aneuploidy increased ROS levels and oxidative DNA damage which induced ATM-dependent p53 activation. This response was abrogated with antioxidant treatment providing evidence that ATM responds to oxidative stress *in vivo*. Loss of ATM in these mice accelerated the onset of tumor development. These studies emphasize that ATM's dual roles in both the DNA damage response and the cellular response to oxidative stress play a part in tumor suppression.

Currently, the factors that promote the progression of NAFLD to NASH and its associated complications including hepatic cirrhosis and hepatocellular are not well understood. Due to the increasing prevalence of NAFLD/NASH and the clear connection to complications including HCC, the overall objective of this study was to establish and characterize an inducible animal model capable of mechanistically evaluating the interaction between hepatic fat accumulation, DNA damage, oxidative stress and NAFLD/NASH disease progression. We hypothesize that increased reactive oxygen species resulting from excess dietary fat contribute to liver disease progression by causing hepatic oxidative stress and DNA damage, resulting in apoptotic cell death and a compensatory hepatic fibrotic response (Figure 3). We tested this by investigating the effects of feeding mice high fat or standard diets for 8 weeks.

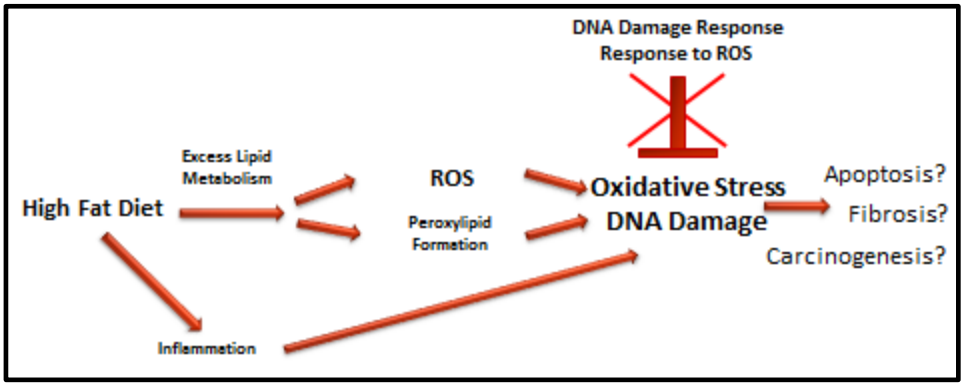

Figure 3: High fat diet feeding leads to hepatic oxidative stress and DNA damage, contributing to fatty liver disease progression. Excess free fatty acids from feeding a high fat diet are metabolized, leading to excess ROS release, which damages hepatocytes, and react with lipid to form highly toxic peroxylipids. This combination leads to hepatic oxidative stress and DNA damage. Inflammation accompanying the lipid accumulation also contributes to the oxidative DNA damage. When DNA damage response pathways and the cellular responses to ROS are intact, this DNA damage is repaired and the oxidative stress on the cell is reduced. However, when these pathways are not intact, this damage and stress may not be processed properly, which could lead to changes in apoptosis, fibrosis, and carcinogenesis.

Our results demonstrate that lipid-laden hepatocytes experience increased oxidative stress and undergo ATM–dependent steatoapoptosis, which occurs independently of detectable H2AX phosphorylation. These findings provide strong evidence that an ATM-mediated DNA damage response contributes to NAFLD progression by promoting apoptosis and fibrosis in the liver.

CHAPTER TWO:

MATERIALS AND METHODS

Animal Husbandry

Atm null mice were used on a FVB/N strain background [58]. $Atm^{+/-}$ mice were intercrossed and progeny were divided into four study groups. In the first and second group, Atm^{+} ($Atm^{+/+}$ and $Atm^{+/-}$) and $Atm^{-/-}$ mice were fed a standard diet (SD) (<0.05% cholesterol, 0% cholic acid, 5% triglyceride; 7012 Harlan Teklad LM-485 Mouse/Rat Sterilizable Diet) and in the third and fourth groups, Atm^{+} and $Atm^{-/-}$ mice were fed a high fat diet (HFD) (1.25% cholesterol, 0.5% cholic acid, 15.5% triglyceride; TD.880511, Harlan, Teklad Lab Animal Diets; "Paigen diet") (Table 1) for eight weeks.

Table 1: Selected nutrient information of the high fat diet.

	% by weight	% kcal
Protein	19.7	20.5
Carbohydrate	40.7	42.4
Fat (half from cocoa butter)	15.8	37.1

Initially, both sexes were assessed separately; however, no differences were seen between the sexes and male and female data were combined (data not shown). Likewise, data from $Atm^{+/-}$ and $Atm^{+/+}$ mice were initially evaluated independently and combined when data indicated there were no differences between these groups. A subset of mice was whole body irradiated with 10 Gy irradiation 8 hours prior to tissue collection. Mice were housed under specific pathogen-free

conditions in an Association for the Assessment and Accreditation of Laboratory Animal Care International accredited facility. Mice received food and water *ad libitum*. All protocols were approved by the Cornell University Institutional Animal Care and Use Committee.

Tissue Harvest and Histopathology

After eight weeks of HFD or SD feeding, mice were euthanized with CO_2. The liver was removed aseptically and weighed. Approximately 30mg of liver was flash frozen in both liquid N_2 and in Tissue-Tek O.C.T. (Sakura Finetek USA) and stored at -80^{o}C. The remainder of the liver was fixed in 10% neutral buffered formalin. Tissues were processed, paraffin embedded, cut into 4-5μ sections, and stained with hematoxylin and eosin. Additional liver sections were stained with Oil Red-O or pico- Sirius Red. Tissues were evaluated by a pathologist blinded to sample identity and study design. Hepatic fat accumulation, inflammation and fibrosis were scored on an ascending 0-4 scale [59].

Quantitative PCR

RNA was extracted from liver samples using the E.Z.N.A Total RNA Kit (Omega) and residual genomic DNA was removed with DNase treatment (Omega), using the manufacturer's recommendations. Total RNA (1-2μg) was used for synthesis of complimentary DNA (qScript cDNA Synthesis Kit; Quanta Biosciences). PerfeCTa SYBR Green FastMix, Low ROX quantitative polymerase chain reaction (PCR) Master Mix (Quanta Biosciences) was used for the quantitative PCR reaction utilizing Applied Biosystems 7500. Gene expression levels were normalized to *Gapdh* expression and quantification was determined via the $\Delta\Delta C_T$ method using

the *Atm*$^{+}$ SD group as the comparative delta value (expression of 1). Error bars represent relative log conversion of standard error as described previously [60]. Primer sets were acquired (Integrated DNA Technologies) as follows: glyceraldehyde-3-phosphate dehydrogenase (Gapdh), p22phox, Puma, Fas, and Fas Receptor.

Immunohistochemistry

Hepatocyte apoptosis was quantified by terminal deoxynucleotidyl transferase-mediated deoxyuridine triphosphate nick-end labeling per manufacturers recommendation (TUNEL; ApopTag Peroxidase In Situ Apoptosis Detection Kit; Millipore). Positive staining was detected with 3,3'-diaminobenzidine tetrahydrochloride (DAB) (Invitrogen) and sections were counterstained with hematoxylin. Liver sections from 5 animals per group were TUNEL stained. For each section, four 20X fields were chosen randomly and the number of TUNEL-positive and TUNEL-negative hepatocytes were quantified.

Immunohistologic detection of phosphorylated H2AX was determined on formalin-fixed, paraffin embedded liver sections. Briefly, sections were deparaffinized and rehydrated. Antigen retrieval was performed by heating the samples to 95^{o}C in 0.25 mM EDTA, pH 8, over 50 minutes. Sections were treated with 3% H_2O_2 for 10 minutes and blocked with 4% bovine serum albumin and 20% Tween in 1XTBS at room temperature and then incubated overnight with primary antibody (1:200 dilution; mouse monoclonal anti-γH2AX antibody; Millipore) at 4^{o}C. Slides were treated with biotinylated secondary antibody for 20 minutes and detected with

Histostain Kit (Invitrogen). Quantification of positive γH2AX hepatocytes was performed in the same manner described for TUNEL staining.

Hydrogen Peroxide, 8-hydroxyguanosine, phospho-ATM and Dihydrorhodamine Imaging and Quantification

Hepatic H_2O_2 levels were detected using the Amplex Red Hydrogen Peroxide/Peroxidase Assay Kit (Molecular Probes). Single cell hepatocyte suspensions were obtained from fresh liver samples and red blood cells were removed using a percol gradient. Reactions containing 50μM Amplex Red reagent, 0.1 U/mL horse radish peroxidase and $1x10^5$ hepatocytes in 50mM sodium phosphate buffer, pH 7.4, were incubated for 30 minutes at 37°C. Fluorescence was measured with a microplate reader using excitation at 530nm and fluorescence detection at 590nm. Absolute H_2O_2 levels were determined in relationship to a standard curve.

Hepatic superoxide was visualized using dihydrorhodamine 123 (DHR) (Molecular Probes/Invitrogen) fluorescent imaging. Hepatocytes were harvested similarly to the H_2O_2 assay. Hepatocytes were washed in 1XPBS, resuspended in media and incubated with 100μL of 25μg/mL solution of DHR in the dark at 37°C for 20 minutes. Hepatocytes were counted and cytospins were performed with $1X10^6$ cells. Images were obtained via confocal microscopy using excitation 596nm, detection at 600-650nm and magnification 63X [61]. Nuclei were stained with 4',6-diamidino-2-phenylindole (DAPI) (Sigma-Aldrich). Mean red fluorescent values were determined by averaging the fluorescence within a set number of pixels placed over 5 areas within a 63X field, 3 fields per sample. Results were expressed on a scale of 0-250.

DNA damage in hepatocytes was detected using an anti-8-hydroxyguanosine (8-OHG) antibody (ab10802, Abcam) and the presence of phosphorylated ATM in hepatocytes was detected using an anti-phospho-Serine1981-ATM (p-ATM) antibody (#200-301-400, Rockland) on frozen liver sections. Liver samples were embedded in Tissue-Tek O.C.T., flash frozen in liquid N_2 and sectioned at 8-10 μM. Sections were fixed in a mixture of 3 parts acetone, one part pure ethanol and washed in 1XPBS. Sections were blocked with casein/10% donkey serum for 20 minutes at room temperature, washed in 1XPBS and then incubated with goat anti-8-OHG antibody (1:100 dilution) for 1 hour at 37^{o}C or mouse anti-p-ATM antibody (1:200 dilution) overnight at 4^{o}C in a humidifying chamber. Sections were washed in 1XPBS and treated with secondary antibodies labeled with Texas Red (1:500 dilution; Jackson ImmunoResearch). Nuclei were labeled with 4',6-diamidino-2-phenylindole (DAPI) (Sigma-Aldrich). For 8-OHG quantification, the percentage of positive 8-OHG cells was calculated over three 80X fields from three different mice per group.

Western Blotting

Cells were harvested and solubilized in RIPA buffer as described previously [62] followed by sonication. Total protein was quantified by Bradford assay, resolved on 6% to 14% SDS-PAGE gels, and subjected to immunoblotting using antibodies against PUMA (Abcam, #ab9643) and anti-beta actin (Sigma, #A5441). Western-blot imaging and quantification was performed using a Versa Doc Imaging System (Bio-Rad Laboratories).

Statistical Analyses

Parametric data were analyzed utilizing one-way analysis of variance followed by Tukey's post-test or by *t* test. Nonparametric data were analyzed by the Mann-Whitney-U test followed by Dunn's post test. *P* values of ≤ 0.05 were considered statistically significant. Data are presented as mean ± standard error of the mean unless otherwise specified. All analyses were made with GraphPad Prism version 5.0 for Windows (GraphPad Software).

CHAPTER THREE:

RESULTS

Hepatic oxidative stress is promoted by high fat diet feeding. Feeding mice a high fat diet with cholesterol and cholic acid leads to increased expression of oxidative stress-related genes [63]. We directly measured oxidative stress associated with excessive fat consumption by harvesting hepatocytes from mice fed either a standard diet (SD) or a high fat diet (HFD) for 8 weeks and performing Amplex Red staining to detect H_2O_2 and dihydrorhodamine (DHR) staining to detect superoxide species. Hepatocytes from mice fed the HFD (n=4) showed significantly elevated levels of H_2O_2 compared to SD fed mice (n=3) (Figure 4A; $*p<0.05$). Superoxide levels, as measured by DHR staining, also were significantly increased in hepatocytes from HFD-fed mice as compared to those from SD-fed animals (Figure 4B and 4C; $*p=0.01$). Quantitative PCR analysis of the NADPH oxidase *p22phox* gene, which plays a central role in superoxide production [63], additionally was performed. Consistent with the H_2O_2 and superoxide quantification, there were significant increases in *p22phox* expression in livers from HFD fed mice compared to those from mice fed SD (Figure 4D; $*p=0.002$). These data indicate that HFD feeding causes increased oxidative stress in hepatocytes.

Figure 4: High fat diet feeding induces hepatic oxidative stress. *Atm*$^{+}$ and *Atm*$^{-/-}$ mice were fed SD or HFD for 8 weeks**.** Hepatocytes were then harvested and analyzed for (A) hydrogen peroxide production (Amplex-Red assay) or (B, C) the presence of superoxide (dihydrorhodamine assay). (A) Comparison of hydrogen peroxide levels showed that hepatocytes from mice fed the HFD (n=4) produced significantly more hydrogen peroxide compared to mice fed the SD (n=3) (**p*<0.05, Student's t-test). Scatter dot plot results are expressed as mean ±SEM. (B) Comparison of the mean red fluorescence of DHR stained livers from SD and HFD fed groups (n=3 for both groups) showed that mice fed the HFD displayed significantly more red fluorescence than the SD fed mice (**p*=0.01, Student's t-test). Results are expressed as mean± SEM on a scale of 0-250. (C) Dihydrorhodamine (DHR) fluorescent staining of hepatocytes harvested from mice fed the SD (top panels) and HFD (lower panels). Scale bars represent 5μm. (D) Quantitative PCR analysis of the NADH/NADPH oxidase *p22 phox* gene from mice fed SD or HFD demonstrated significant increases in the HFD group compared to the SD group (**p*=0.002, Student's t-test). Gene expression was normalized to *Gapdh* expression and was compared by the $\Delta\Delta C_T$ method.

Figure 4

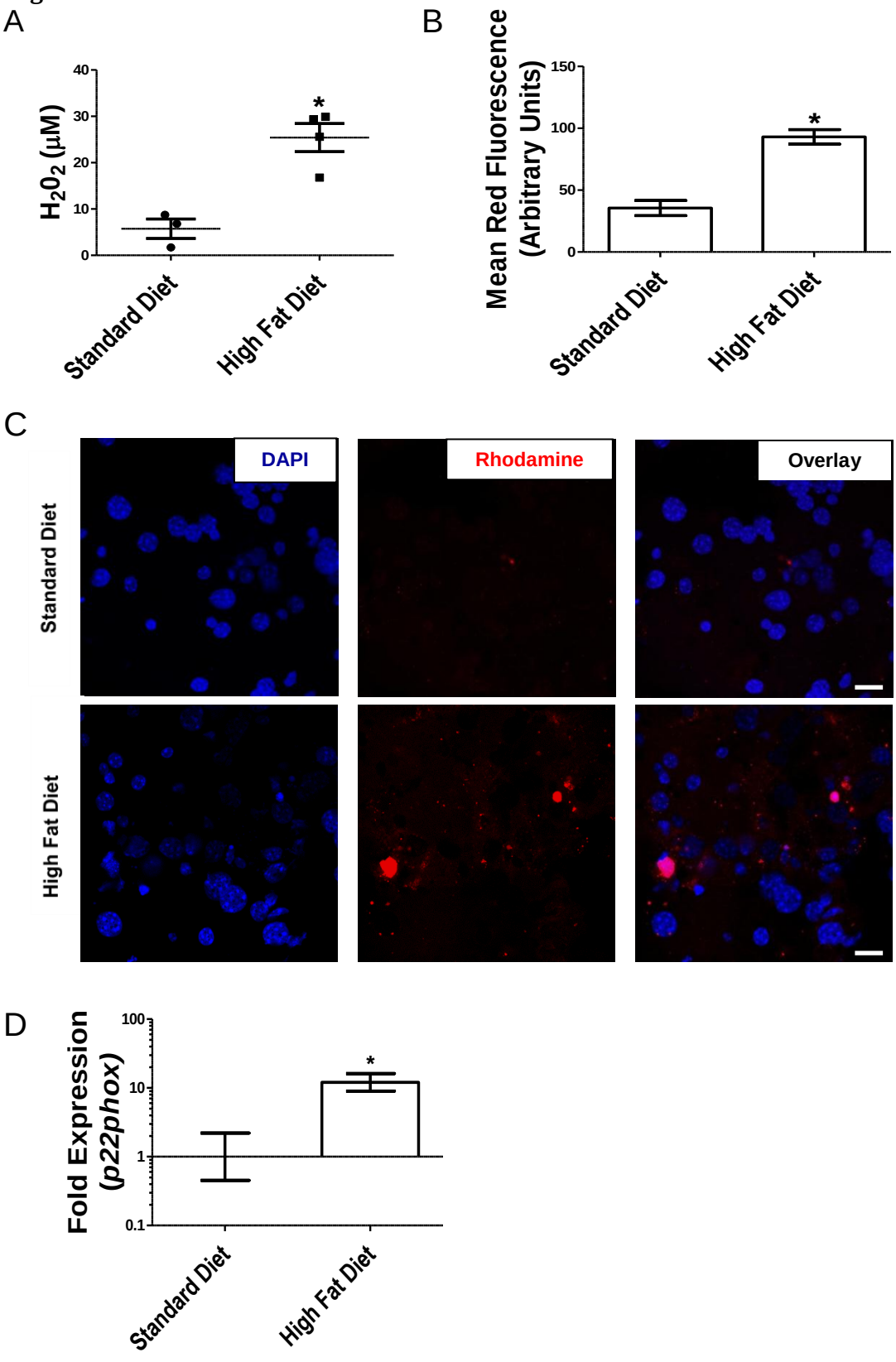
A
H_2O_2 (μM)
40
30
20
10
0
*
Standard Diet
High Fat Diet
B
Mean Red Fluorescence (Arbitrary Units)
150
100
50
0
*
Standard Diet
High Fat Diet
C
DAPI
Rhodamine
Overlay
Standard Diet
High Fat Diet
D
Fold Expression (p22phox)
100
10
1
0.1
*
Standard Diet
High Fat Diet

High fat diet feeding induces hepatomegaly, steatohepatitis and ATM activation, and promotes hepatic fibrosis in an *Atm*-dependent manner. ATM activation plays an important role in the cellular response to ROS, and A-T patients display increased sensitivity to oxidative stress [13,42,64]. We therefore assessed ATM pathway activation in mice following HFD feeding via immunofluorescent staining of liver sections using an antibody that detects phosphorylated, active ATM (pS1987 of mouse ATM, corresponding to pS1981 of human ATM) [49]. Hepatocytes from Atm^{+} ($Atm^{+/+}$ and $Atm^{+/-}$) HFD fed mice displayed both nuclear and cytoplasmic foci containing p-ATM, while hepatocytes from Atm^{+} SD fed mice did not, confirming hepatic ATM activation in the Atm^{+} HFD fed group (Figure 5A). The majority of the foci appeared to be localized to the periphery of the nucleus. The detection of HFD-induced ATM phosphorylation was specific, as no staining was observed in $Atm^{-/-}$ hepatocytes from mice fed either diet. We next tested the ability of *Atm*-deficient mice to respond to HFD feeding. Livers were examined grossly and microscopically after 8 weeks of feeding SD or HFD to determine if HFD feeding induced hepatic changes consistent with NAFLD. For all measures described below, we observed no significant differences between $Atm^{+/+}$ and $Atm^{+/-}$ mice and therefore in most cases present combined data for these genotypes under the label Atm^{+}. Irrespective of *Atm* status, there was 100% prevalence of fatty liver development in mice fed the HFD (n=22), whereas all mice fed the SD (n=23) had grossly normal livers (Figure 5B). Mice fed the HFD also had marked increases in liver weight (Figure 5C; $*p< 0.0001$), but not in total body weight (Figure 5D) compared to mice fed the SD, indicating that the HFD induced hepatic fat accumulation independent of obesity. Consistent with previous reports [58,65,66] $Atm^{-/-}$ mice had slightly lower body weights compared to Atm^{+} mice regardless of diet (Figure 5D). Upon both H&E and Oil-red-O staining, hepatocytes from HFD fed $Atm^{+/+}$ and $Atm^{-/-}$ mice displayed

marked cellular hypertrophy and both microvesicular and macrovesicular steatosis (Figure 6A). In contrast, there was no abnormal hepatic fat accumulation in mice fed the SD. Further, mice fed the HFD had significantly higher fatty liver scores compared to SD fed controls irrespective of *Atm* genotype (Figure 6B,*$p < 0.0001$). These data demonstrate that 8 weeks of HFD feeding produced marked hepatic steatosis consistent with NAFLD in both *Atm*-expressing and *Atm*-deficient mice.

Figure 5: High fat diet feeding induces grossly evident fatty liver without fat accumulation in other tissues: *Atm*$^{+}$ and *Atm*$^{-/-}$ mice were fed SD or HFD for 8 weeks**.** Liver weight, body weight, and liver appearance were evaluated post euthanasia. Hepatocytes were then harvested and analyzed by immunofluorescence. (A) Frozen sections of livers from *Atm*$^{+/+}$ mice fed SD or HFD and *Atm*$^{-/-}$ mice fed the HFD were labeled with anti-phospho-ATM (p-ATM) antibody and examined by confocal microscopy. Blue fluorescence signals represent DAPI stained nuclei and positive p-ATM foci fluoresce red. Scale bars represent 2.5 μm. (B) Representative images of liver from SD and HFD groups at the time of euthanasia. Scale bars represent 0.5cm. (C) Comparison of liver weights and (D) total body weights of mice of the indicated genotypes after 8 weeks of HFD or SD feeding showed that mice fed the HFD had marked increases in liver weight compared to mice fed the SD (*p< 0.0001, Student's t-test). Results are expressed as mean ± SEM.

Figure 5

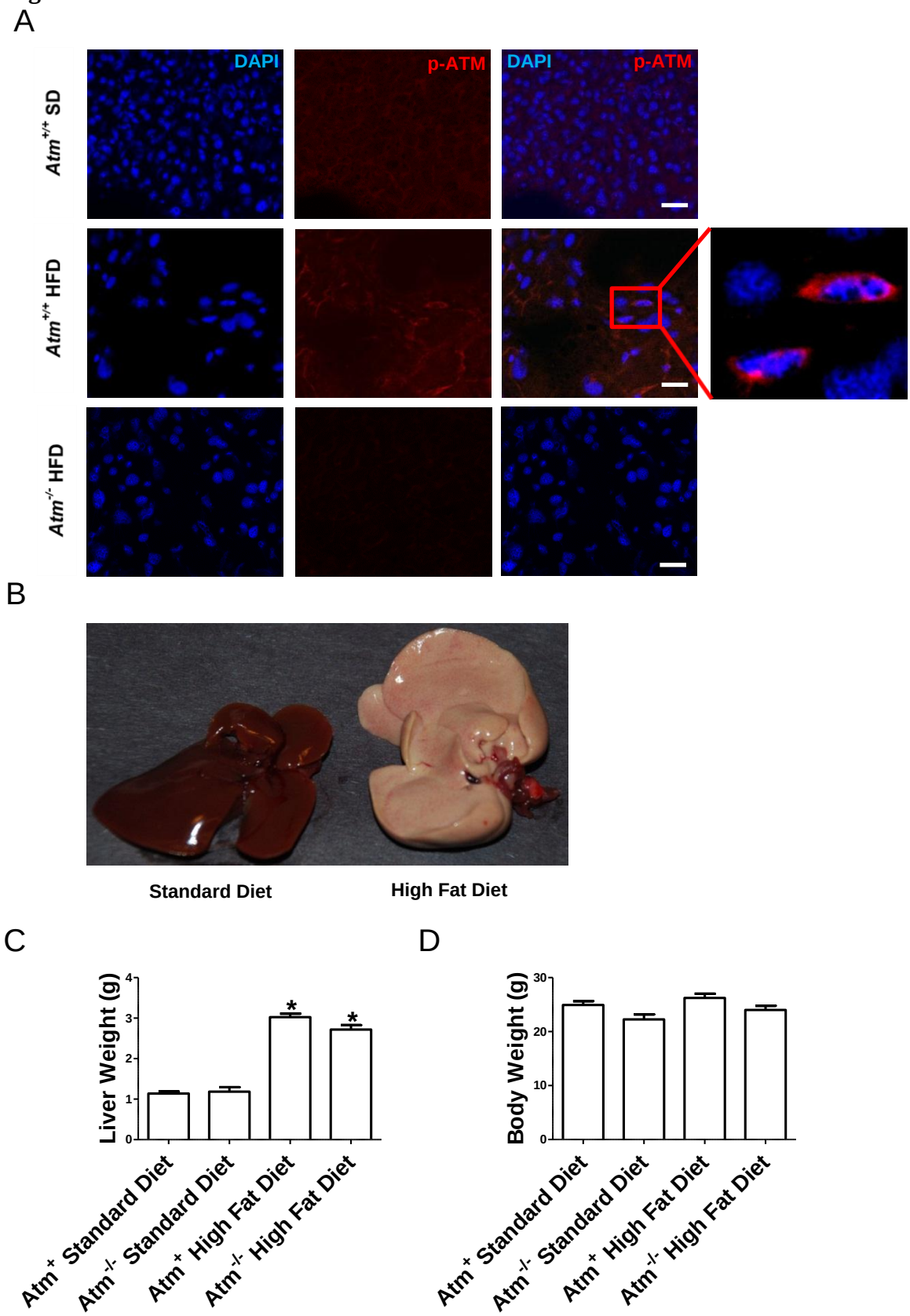
A
DAPI
p-ATM
DAPI
p-ATM
Atm+/+ SD
Atm+/+ HFD
Atm-/- HFD
B
Standard Diet
High Fat Diet
C
Liver Weight (g)
0
1
2
3
4
*
*
Atm+ Standard Diet
Atm-/- Standard Diet
Atm+ High Fat Diet
Atm-/- High Fat Diet
D
Body Weight (g)
0
10
20
30
Atm+ Standard Diet
Atm-/- Standard Diet
Atm+ High Fat Diet
Atm-/- High Fat Diet

Figure 6: High fat diet feeding induces hepatic steatosis and hepatitis regardless of *Atm* status, but leads to more fibrosis in *Atm*$^{+}$ livers. H&E (A, first row, scale bars represent 20μm), Sirius red (A, second row, scale bars represent 20μm) and Oil-Red-O (A, third row, scale bars represent 10μm) sections from mice fed SD (n=20) or HFD (n=25) for 8 weeks were scored blindly on a scale of 0-4 for fat accumulation (B), inflammation (C) and fibrosis (D). Results are expressed as mean ± SEM. Statistical values were obtained using Mann-Whitney-U test followed by Dunn's post test. Comparison of scores between HFD and SD fed mice showed that regardless of *Atm* status, mice fed HFD had significantly higher fatty liver (B;*$p< 0.0001$), inflammation (C; *$p< 0.05$) and fibrosis (D; **$p< 0.05$) scores when compared to mice fed SD. Additionally, *Atm*$^{+}$ mice fed the HFD developed significantly higher fibrosis scores (D, ***$p< 0.05$) compared to *Atm*$^{-/-}$ mice. Differences in fibrosis were highlighted by fewer Sirius red positive foci in *Atm*$^{-/-}$ mice (A, second row, arrows). H&E staining of livers from SD fed *Atm*$^{+}$ and *Atm*$^{-/-}$ mice revealed histologically normal liver, while mice of both genotypes, when fed the HFD, displayed cellular hypertrophy and accumulation of microvesicular (arrow head) and macrovesicular (thin arrows) steatosis, and portal inflammation (thick arrows). Mice fed the SD did not develop inflammation. Oil Red-O staining confirmed the presence of marked lipid accumulation in HFD fed livers.

Figure 6

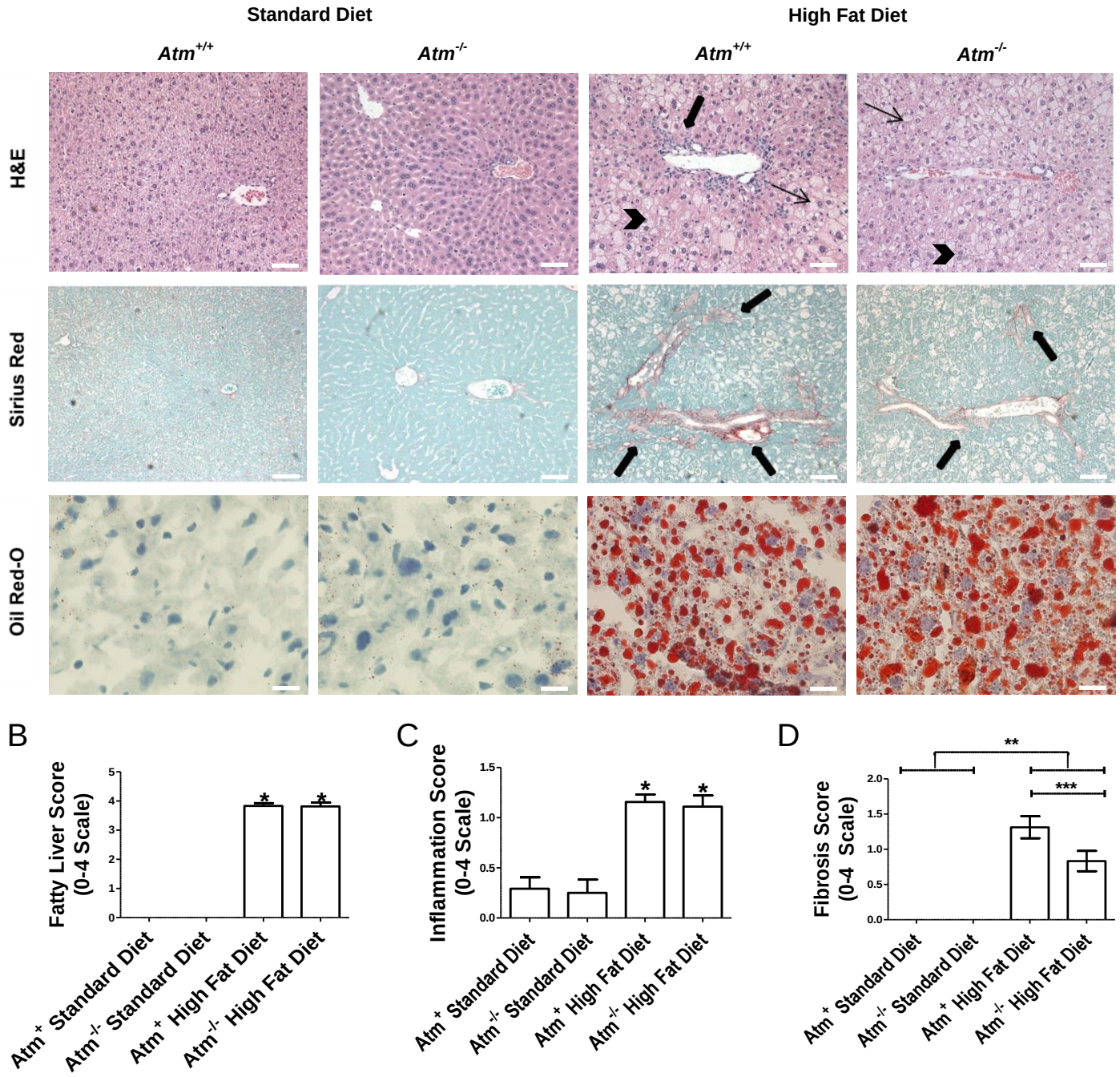
A
Standard Diet
High Fat Diet
Atm+/+
Atm-/-
Atm+/+
Atm-/-
H&E
Sirius Red
Oil Red-O
B
Fatty Liver Score (0-4 Scale)
0
1
2
3
4
5
*
*
Atm+ Standard Diet
Atm-/- Standard Diet
Atm+ High Fat Diet
Atm-/- High Fat Diet
C
Inflammation Score (0-4 Scale)
0.0
0.5
1.0
1.5
*
*
Atm+ Standard Diet
Atm-/- Standard Diet
Atm+ High Fat Diet
Atm-/- High Fat Diet
D
Fibrosis Score (0-4 Scale)
0.0
0.5
1.0
1.5
2.0
**
***
Atm+ Standard Diet
Atm-/- Standard Diet
Atm+ High Fat Diet
Atm-/- High Fat Diet

Additional hepatic phenotypes resulting from 8 weeks of HFD feeding were evaluated based on H&E staining and pico-sirius red staining for collagen. Livers from both Atm^{+} and $Atm^{-/-}$ mice fed the HFD demonstrated moderate, predominantly peri-portal, mixed inflammatory cell infiltrates (Figure 6A). In contrast, there were no hepatic inflammatory lesions in mice fed the SD. Further, all mice fed the HFD, regardless of genotype, had significantly higher inflammation (Figure 6C, $*p< 0.05$) and fibrosis (Figure 6D, $**p< 0.05$) scores when compared to mice fed the SD. Notably, Atm^{+} HFD fed mice developed significantly more fibrosis than $Atm^{-/-}$ mice (Figure 6D, $***p< 0.05$). Differences in fibrosis development were highlighted by fewer and smaller pico-sirius red-positive foci in the livers of $Atm^{-/-}$ mice as compared to those of Atm^{+} mice (Figure 6A). These data demonstrate that 8 weeks of HFD feeding produces marked steatohepatitis regardless of *Atm* status and that subsequent fibrosis is dependent, at least in part, on ATM.

High fat diet feeding induces oxidative nucleic acid damage but limited histone H2AX phosphorylation. To understand the basis for the effects of *Atm* deficiency on HFD- induced liver pathology we evaluated whether *Atm* loss affects ROS levels in HFD fed mice. To a similar extent as was observed in Atm^{+} mice (Figure 4), HFD feeding of $Atm^{-/-}$ mice caused increased H_2O_2 and superoxide accumulation relative to SD fed mice (Figure 7A, $*p=0.004$; 7B, $*p=0.01$). Levels of 8-hydroxyguanosine (8-OHG), an oxidized nucleotide and marker of oxidative nucleic acid damage were then quantified to determine if the elevated oxidative stress in fatty livers resulted in hepatocyte DNA damage. There was minimal staining for 8-OHG in the SD group while there were multiple 8-OHG positive aggregates within the nuclei and cytoplasm of hepatocytes from HFD fed mice (Figure 7C). In some nuclei, 8-OHG appeared to be localized to

the periphery of the nucleus. Quantification of 8-OHG positive cells showed that there were significantly more positive cells in the Atm^{+} and $Atm^{-/-}$ groups fed the HFD than in mice fed the SD (Figure 7D; *p= 0.001). There was no significant difference between Atm^{+} and $Atm^{-/-}$ HFD fed groups. These findings indicate that the HFD causes oxidative nucleic acid damage in both *Atm*-expressing and *Atm*-deficient mice.

To determine the nature and extent of the DNA damage response induced by HFD feeding, we performed immunohistochemistry on liver sections from HFD and SD fed groups and quantified the levels of γ-H2AX, the phosphorylated form of histone H2AX which occurs in response to DNA DSBs [67]. In contrast to our earlier observations of HFD feeding-induced ATM phosphorylation (Figure 5A), there was minimal positive staining for H2AX phosphorylation in hepatic nuclei from mice of all experimental groups (Figure 7E; *p<0.0001; 7F; 7H; 7I). Importantly, significant increases in γ-H2AX staining were detected in liver sections from control mice treated with ionizing radiation (Figure 7E and 7G). Overall, these data demonstrate that there is DNA damage in HFD fed hepatocytes without substantial phosphorylation of H2AX.

Figure 7: High fat diet feeding increases hepatic nucleic acid damage but does not induce detectable phosphorylation of histone H2AX. (A-B) Hepatocytes were harvested from mice of the indicated genotypes and analyzed for hydrogen peroxide production (amplex-red assay) and the presence of superoxide (dihydrorhodamine assay). The data for Atm^{+} mice are identical to those shown in Figure 4. (A) Hepatocytes from mice fed the high fat diet (n=4/group) produced significantly more hydrogen peroxide compared to standard diet fed mice (n=3) (**p*=0.004*)*. Scatter dot plot results are expressed as mean ±SEM. (B) Comparison of the mean red fluorescence of DHR stained livers from standard diet, and Atm^{+} and $Atm^{-/-}$ high fat diet fed groups (n=3/groups) showed that, regardless of genotype, mice fed the high fat diet displayed significantly more red fluorescence than the standard diet fed mice (**p*=0.01). There was no difference in mean red fluorescence between high fat diet groups. Mean fluorescent values were determined by averaging the fluorescence within a set number of pixels placed over 5 areas within a 63X field, 3 fields per sample. Results are expressed as mean± SEM on a scale of 0-250. (C) Frozen sections of livers from mice fed SD (right) or the HFD (left) were labeled with anti- 8-hydroxyguanosine (8-OHG) antibody and examined by confocal microscopy. Blue fluorescence signals represent DAPI stained nuclei and positive 8-OHG foci fluoresce red. Scale bars represent 2.5 μm. (D) Quantitation of the experiment described in (C) highlights that there were significantly more 8-OGH positive nuclei per 80X field in the Atm^{+} and $Atm^{-/-}$ groups fed the HFD than in the Atm^{+} group fed the SD (**p*= 0.001, Student's t-test) (n=3 in each group). Results are expressed as mean± SEM. The percentage of 8-OHG positive nuclei out of total DAPI positive nuclei was calculated over three 80X fields. (E) Immunohistochemistry was performed to identify phosphorylated histone H2AX in liver sections from HFD and SD fed mice of the indicated genotypes (n=3/group) and revealed that there was minimal staining in these groups while there was significantly more staining detected in Atm^{+} livers treated with 10 Gy IR regardless of genotype (**p*<0.0001, Student's t-test). Data on graph represent mean ± SEM. (F-I) Representative images of liver sections stained with anti-γH2AX antibody (brown nuclei, arrow) from (F) $Atm^{+/+}$ standard diet, (G) $Atm^{+/+}$ irradiated and (H) $Atm^{+/+}$ high fat diet and (I) $Atm^{-/-}$ high fat diet fed groups. Sections were counterstained with hematoxylin. Quantification is shown in Figure 7E. Scale bars represent 15μm.

Figure 7

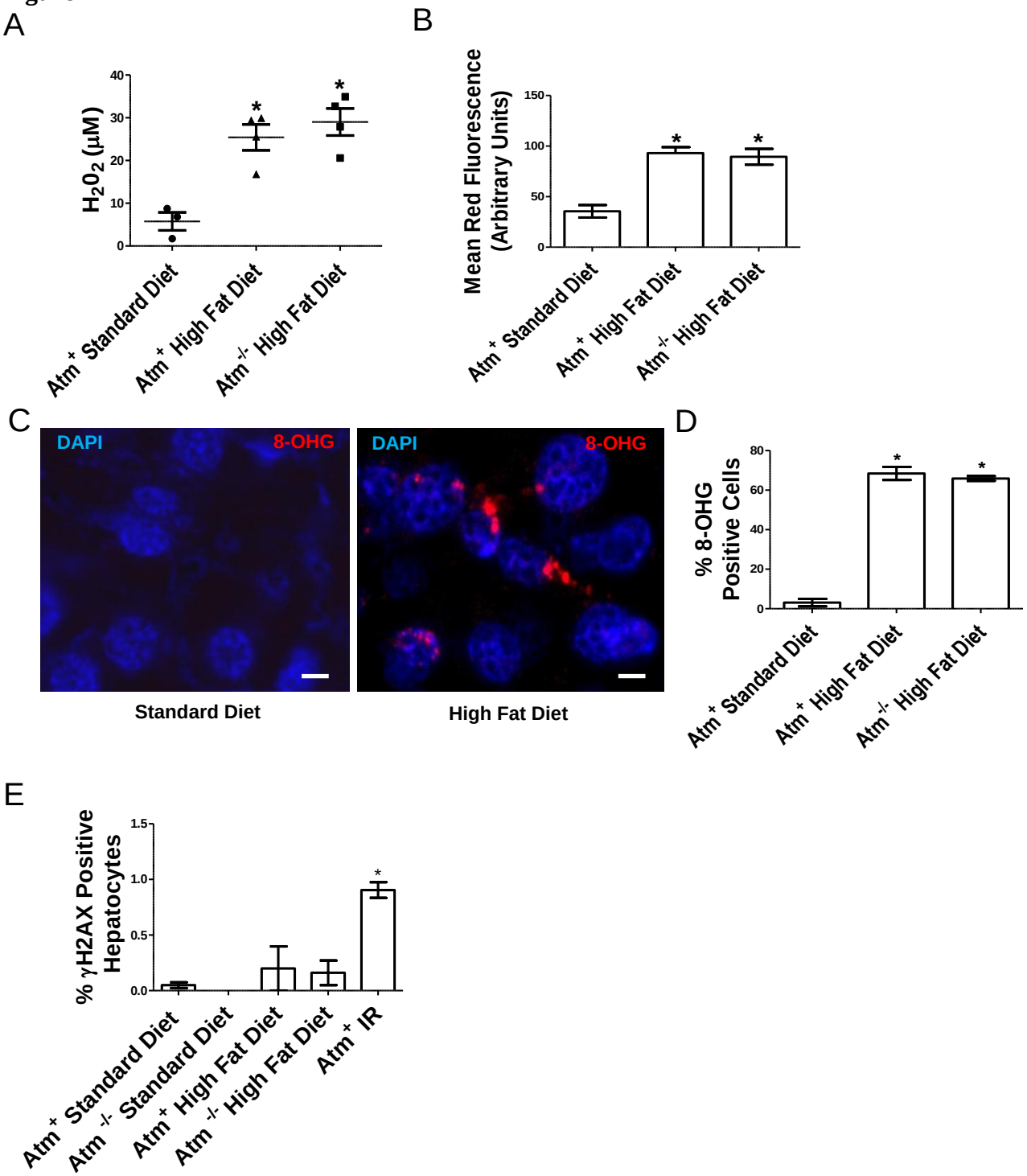
A
H_2O_2 (μM)
40
30
20
10
0
Atm + Standard Diet
Atm + High Fat Diet
Atm -/- High Fat Diet
B
Mean Red Fluorescence (Arbitrary Units)
150
100
50
0
Atm + Standard Diet
Atm + High Fat Diet
Atm -/- High Fat Diet
C
DAPI
8-OHG
DAPI
8-OHG
Standard Diet
High Fat Diet
D
% 8-OHG Positive Cells
80
60
40
20
0
Atm + Standard Diet
Atm + High Fat Diet
Atm -/- High Fat Diet
E
% γH2AX Positive Hepatocytes
1.5
1.0
0.5
0.0
Atm + Standard Diet
Atm -/- Standard Diet
Atm + High Fat Diet
Atm -/- High Fat Diet
Atm + IR

Figure 7 (Continued)

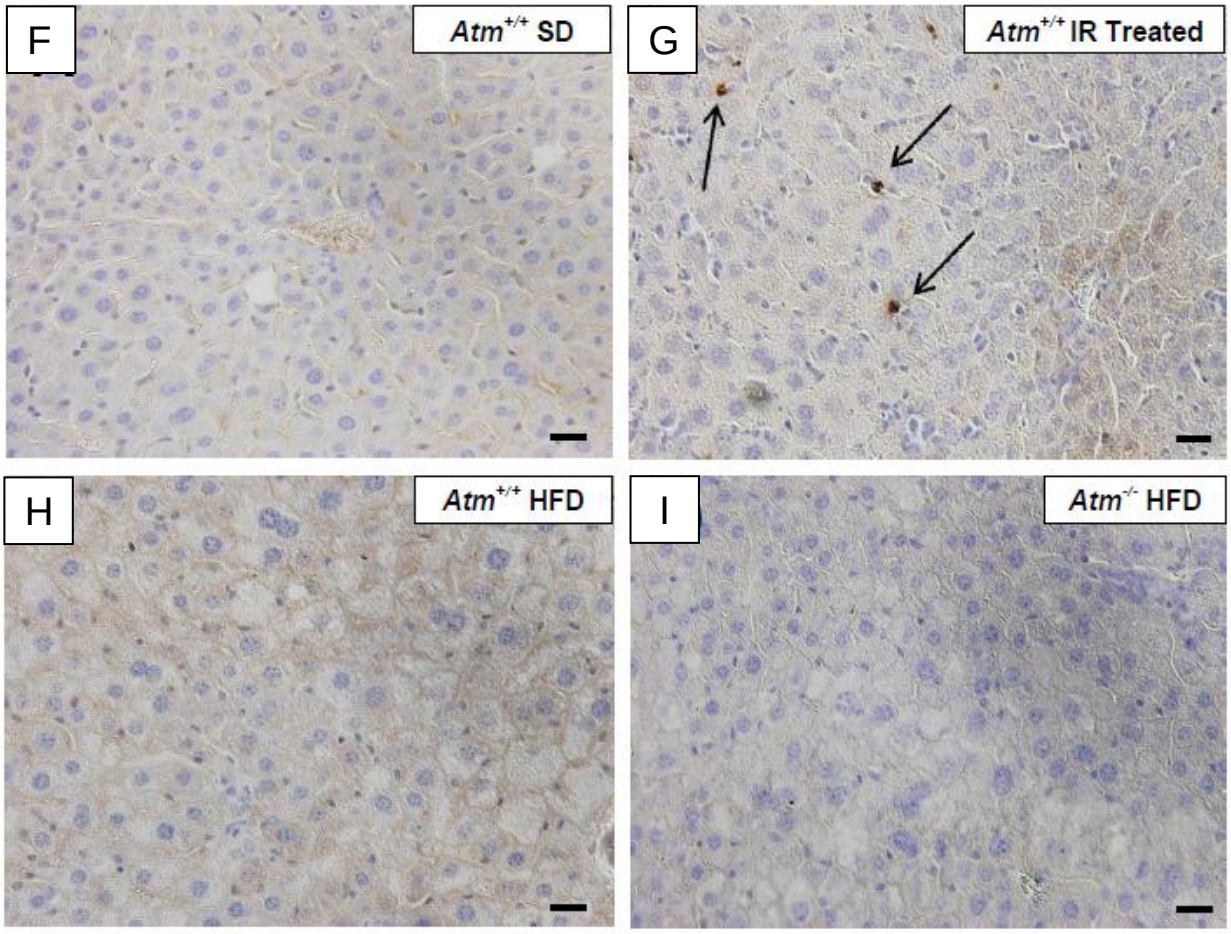

High fat diet feeding increases *Atm*-dependent steatoapoptosis. One of the outcomes of ATM pathway activation is apoptosis [68], and steatoapoptosis is important in fatty liver progression [19,21,22]. The induction of apoptosis by HFD feeding was evaluated by terminal uridine deoxynucleotidyl transferase dUTP nick end labeling (TUNEL) staining of liver sections (n=5-10/group; Figure 8 C-F). TUNEL staining detects DNA fragmentation, a characteristic feature of apoptotic cells. HFD groups contained significantly more TUNEL-positive hepatocytes compared to SD groups, which exhibited minimal positive staining (Figure 8A; $*p \leq 0.0001$). Notably, among the HFD fed mice, Atm^{+} hepatocytes underwent significantly more apoptosis than those from $Atm^{-/-}$ mice (Figure 8A; $**p<0.001$). To dissect the molecular basis for this ATM-dependent apoptotic response to HFD feeding, we used quantitative PCR to measure the expression of the DNA damage-responsive, pro-apoptotic gene *Puma* [69]. HFD fed Atm^{+} mice (n=12) had increased *Puma* expression when compared to all other groups, including HFD fed *Atm*-deficient mice (n=10-12/group), indicating that PUMA is induced after HFD feeding through a mechanism that requires ATM (Figure 8B; $*p<0.01$). HFD feeding similarly resulted in increased PUMA protein levels as measured by immunoblotting of livers from Atm^{+} HFD fed mice, and this induction of PUMA was greatly reduced in samples from *Atm*-deficient mice (Figure 8G). There were also appreciable increases in *Fas receptor* expression, a component of the extrinsic pathway of apoptosis, between SD and HFD groups, but the levels were nearly identical between Atm^{+} and $Atm^{-/-}$ HFD groups (Figure 8H). Together, these data indicate that HFD feeding induces ATM-dependent upregulation of PUMA and hepatocyte apoptosis.

Figure 8: High fat diet feeding induces *Atm*-dependent steatoapoptosis: (A) TUNEL staining to identify apoptotic cells in liver sections from mice of the indicated group (n=5-10/group) was quantified and revealed that HFD groups, regardless of genotype, contained significantly more TUNEL-positive hepatocyte nuclei compared to the SD (*p<0.0001, Student's t-test). Comparison of TUNEL quantification from HFD fed mice showed that hepatocytes from Atm^{+} mice underwent significantly more apoptosis than those from $Atm^{-/-}$mice (**p<0.001). Data represent mean ± SEM. (B) Quantitative PCR analysis of the pro-apoptotic gene *Puma* from Atm^{+} and $Atm^{-/-}$ mice fed either SD or HFD for 8 weeks demonstrated that the Atm^{+} HFD mice (n=12) had increased *Puma* expression when compared to all other groups (n=10-12/group) (*p<0.01, Student's t-test). (C-F) Representative images of TUNEL stained (brown nuclei, arrow) liver sections from $Atm^{+/+}$ and $Atm^{-/-}$ mice from standard and high fat diet fed groups demonstrated that there were minimal TUNEL positive hepatic nuclei when the mice were fed the standard diet, while there were TUNEL positive apoptotic nuclei when the mice were fed the high fat diet. Sections were counterstained with hematoxylin. Quantification is shown in Figure 5A. Scale bars represent 7μm. (G) Total protein lysates were prepared from frozen liver section after feeding SD or HFD and immunoblotted for PUMA. Liver lysates from untreated (-IR) or ionizing radiation treated (+IR, 2 hours post-5Gy) mice were used as negative and positive controls respectively. β-ACTIN was used as a loading control. (H) Quantitative PCR analysis of the *Fas Receptor (CD95)* gene expression in livers from standard diet (n=5), Atm^{+} high fat diet (n=6) and $Atm^{-/-}$ high fat diet (n=5) groups demonstrated that regardless of genotype, there was minimal increase in *Fas Receptor* expression in high fat diet fed hepatocytes when compared to mice fed the standard diet (via t-test).

Figure 8

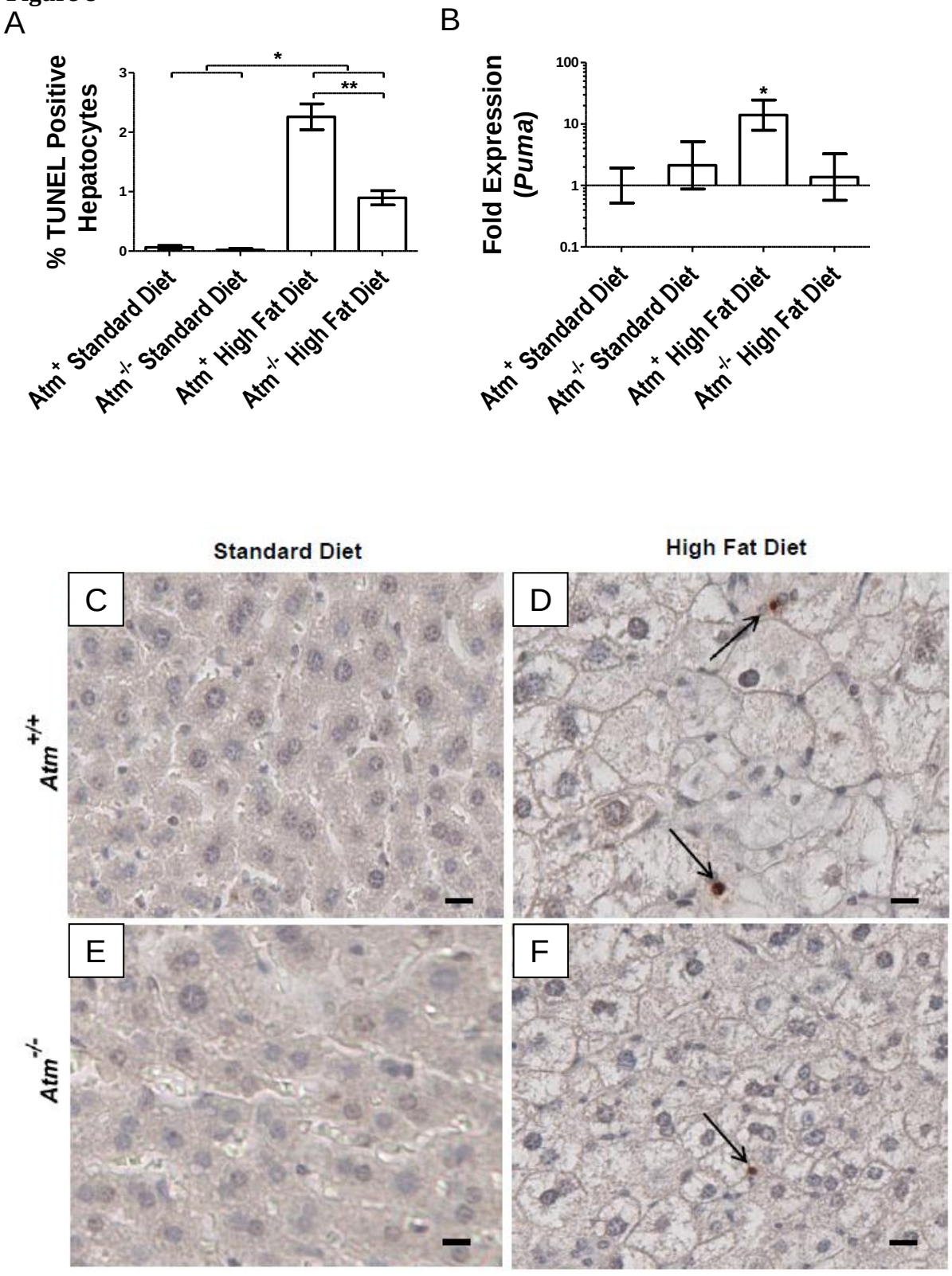
A
% TUNEL Positive Hepatocytes
3
2
1
0
*
**
Atm+ Standard Diet
Atm-/- Standard Diet
Atm+ High Fat Diet
Atm-/- High Fat Diet
B
Fold Expression (Puma)
100
10
1
0.1
*
Atm+ Standard Diet
Atm-/- Standard Diet
Atm+ High Fat Diet
Atm-/- High Fat Diet
Standard Diet
High Fat Diet
C
D
E
F
Atm+/+
Atm-/-

Figure 8 (Continued)

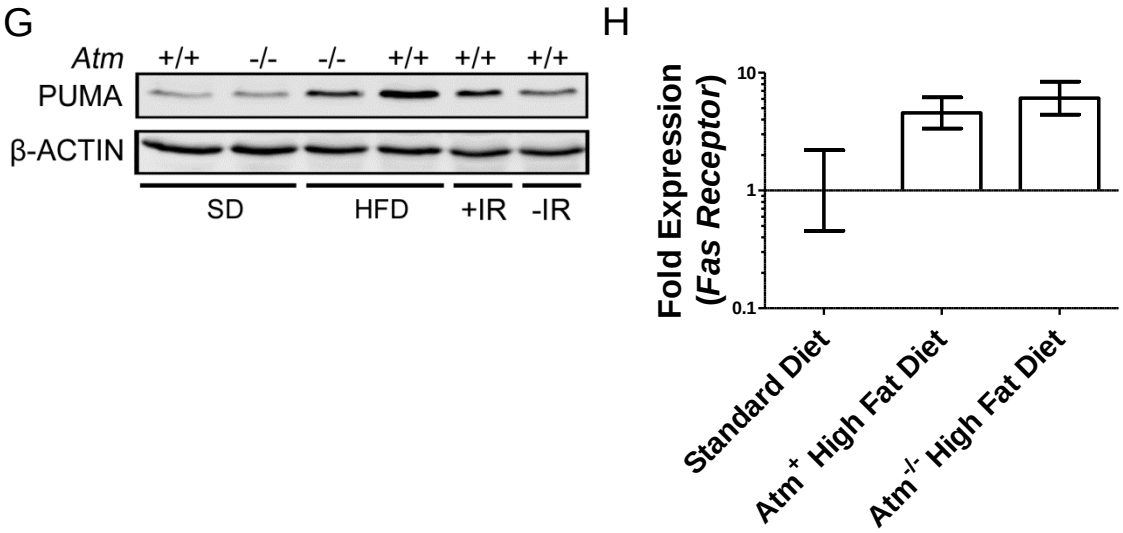

CHAPTER FOUR:

CONCLUSIONS

NAFLD represents an array of hepatic lesions ranging from benign steatosis to hepatic inflammation and cirrhosis. Because of the increasing prevalence of this disease, a more thorough understanding of the factors involved in NAFLD progression is warranted. This study investigated the roles of ATM, a protein kinase involved in maintaining genomic stability, in a diet-induced model of NAFLD/NASH. Other models of NASH use genetic defects, chemical agents, or nutrient depletion to induce steatohepatitis and hepatic fibrosis. Nutritional models, such as sucrose- and fructose-rich diets, cause only minimal hepatic steatosis and inflammation [63]. Conversely, the diet used in this study closely recreated the NAFLD phenotype of steatohepatitis and fibrosis by coupling high fat with cholesterol and cholic acid. Fat accumulation elsewhere in the body was not observed, presumably due to the fat source and the relatively short time period mice were fed the HFD.

Eight weeks of HFD feeding caused hepatic phenotypes in mice consistent with NAFLD, including hepatic steatosis and oxidative stress indicated by elevated levels of ROS and increased expression of *p22phox,* a gene encoding a subunit of NADPH oxidase. Hepatic lipid accumulation is considered an initiating factor in NAFLD pathogenesis and renders hepatocytes susceptible to oxidative stress. High levels of oxidative stress correlate with increasing severity of liver disease in humans [5]. In this study, we showed that HFD-induced steatohepatitis and hepatic oxidative stress were present in both Atm^{+} and $Atm^{-/-}$ mice, which recapitulates essential

components of NAFLD/NASH and creates a hepatic environment ideal to study the effects of *Atm* loss on NAFLD progression.

Chronic liver injury results in fibrosis [36,70]. After 8 weeks of HFD feeding, Atm^{+} mice exhibited more hepatic fibrosis than $Atm^{-/-}$ mice. Interestingly, the same trend was observed for hepatic apoptosis, with Atm^{+} mice exhibiting more hepatocyte apoptosis than $Atm^{-/-}$ mice after chronic HFD feeding. This is consistent with data indicating that apoptosis contributes to fibrosis in NAFLD/NASH progression as well as *in vitro* studies which suggest a direct link between hepatocyte apoptosis and fibrosis [20,21,22,71]. Although the precise mechanistic details have not been fully resolved, available data indicate that apoptosis and cell clearance stimulate quiescent hepatic stellate cells, triggering their transformation to a myofibroblast phenotype and subsequent extracellular matrix deposition [12,72].

Differences in fibrosis and steatoapoptosis between HFD fed Atm^{+} and $Atm^{-/-}$ mice correlated with expression levels of the pro-apoptotic gene *Puma* at both the mRNA and protein levels. Excessive ROS production, as seen in this model, may induce apoptosis via various pathways, including the intrinsic pathway of apoptosis which involves PUMA signaling [12,73]. Recent studies identify PUMA as an important factor in hepatocyte steatoapoptosis, and PUMA inhibition or deficiency leads to decreased hepatic apoptosis [25,27,32,73]. Moreover, hepatic *Puma* expression is increased in NASH patients as compared to expression levels in NAFLD or healthy patients, implicating PUMA in fatty liver disease progression, likely through functions related to steatoapoptosis and fibrosis formation [19,25]. *Puma* activation relies primarily on the

DNA damage inducible transcription factor p53 [73]. ATM is an upstream activator of p53, linking ATM to PUMA-mediated apoptosis in a manner consistent with the ATM-dependent upregulation of *Puma* expression in this model. We also evaluated components of the extrinsic pathway of apoptosis, including *Fas* and *Fas receptor*, via quantitative PCR. There were appreciable increases in *Fas receptor* expression between SD and HFD groups, but the levels were nearly identical between Atm^{+} and $Atm^{-/-}$ HFD groups (Figure 8H). Further, there was no detectable expression of *Fas* ligand in any treatment group (data not shown). Although we cannot entirely rule out involvement of the extrinsic pathway of apoptosis in high fat mediated apoptotic cell death, it does not appear to account for differences observed in hepatocyte death between HFD fed Atm^{+} and $Atm^{-/-}$ mice.

One of the most common causes of hepatic genomic instability is ROS-induced DNA damage [38,74]. In this study chronic HFD feeding caused oxidative nucleic acid damage regardless of *Atm* status as evidenced by the similar percent of 8-OHG-positive cells in HFD fed Atm^{+} and $Atm^{-/-}$ mice. Interestingly, phosphorylation of histone H2AX, a marker of DNA DSBs, was not detectably induced in the HFD groups. γ-H2AX positive hepatocytes were present in IR treated control samples, demonstrating that the immunohistochemical assay for γ-H2AX was functional. Thus, hepatocytes are capable of phosphorylating H2AX but do not do so to a detectable level in response to HFD feeding. Studies show that ROS-induced ATM activation can occur in the absence of DNA DSBs, and this is associated with phosphorylation of only a subset of ATM targets that does not include H2AX [41,42]. Taken together, these data suggest that ATM-mediated fatty liver phenotypes may be the result of an oxidative stress response rather than the classical γ-H2AX associated signaling pathway. The observation of phospho-

ATM in the cytoplasm of fat-laden hepatocytes provides further support for a ROS mediated mechanism of ATM activation [41]. Within the nucleus, both 8-OHG and p-ATM seemed to be more abundant at the nuclear periphery. One hypothesis to explain the observed localization of 8-OHG is that the low permeability of reactive oxygen species limits their mobility through the nuclear membrane, thus creating the most extensive oxidative damage at the nuclear periphery [75]. The observed staining patterns also may relate to previous *in vitro* studies demonstrating that oxidative damage preferentially occurs in heterochromatin, which is predominantly located in the nuclear periphery, and that ATM is critical in repairing this damage [76].

NASH carries a risk of HCC formation. It is well established that apoptosis promotes hepatic fibrosis, and both are key risk factors for HCC development, with hepatic fibrosis and cirrhosis being present in 80-90% of patients with HCC [36,37,77]. In this study, steatoapoptosis and fibrosis were observed at highest levels in Atm-expressing HFD fed mice, indicating that the ATM pathway promotes both during hepatic lipid accumulation. Although apoptosis is generally regarded as a tumor suppressing mechanism that clears damaged cells at risk of undergoing malignant transformation, there also are several examples of tumor promoting effects of apoptosis, including in HCC [24]. Here, the ultimate effect of reduced fibrosis and apoptosis on tumor development could not be determined because *Atm*$^{-/-}$ mice develop thymic lymphoma at 3-4 months of age [58,65,66] preventing long-term evaluation of liver carcinogenesis. However, based upon the recognized influences of apoptosis and fibrosis during HCC development, it is reasonable to hypothesize that the observed *Atm*-dependent increases in these processes could promote hepatic carcinogenesis. Therefore, pharmacological inhibition of ATM may be beneficial to limit fibrosis formation and NAFLD progression.

Figure 9

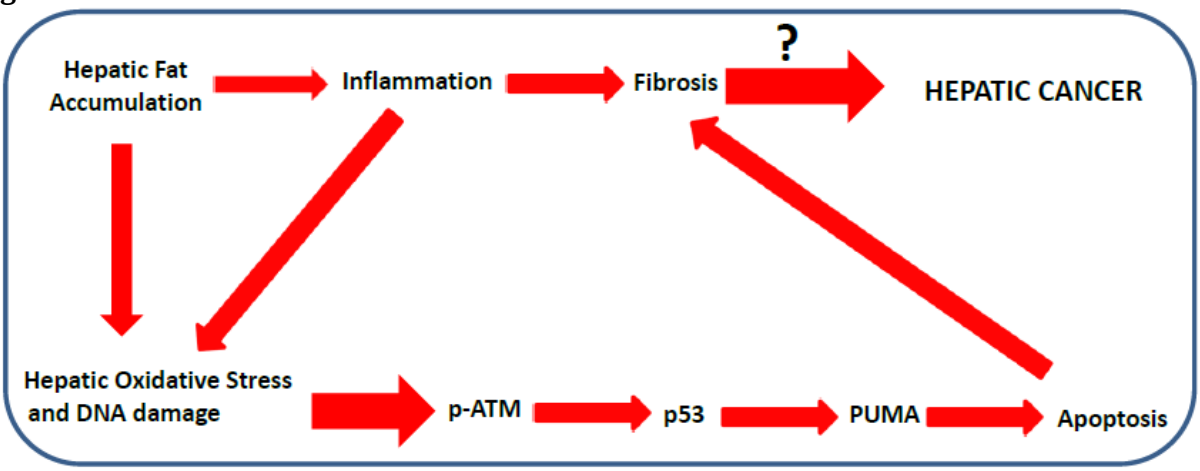

Figure 9: Hepatic fat accumulation triggers oxidative stress and activation of an ATM-mediated DNA damage response, resulting in steatoapoptosis and hepatic fibrosis: ATM is activated during high fat diet feeding, resulting in upregulation of pro-apoptotic PUMA, leading to increased hepatic apoptosis and compensatory fibrosis formation. *Atm*-dependent increases in these processes could promote hepatic carcinogenesis.

Summary and Future Directions

In summary, these findings suggest that hepatic fat accumulation triggers oxidative stress and activation of an ATM-mediated DNA damage response, resulting in steatoapoptosis and hepatic fibrosis (Figure 9). Human trials have been inconclusive regarding effective therapy for NAFLD, including antioxidants, insulin sensitizers, weight loss, or a combination of these modalities [78,79]. However, our data suggest that modulation of ROS levels and ATM activation may provide novel therapeutic targets to prevent the progression of NAFLD. The mouse model described here provides a system for further experimental evaluation of how candidate therapeutics like the antioxidants NAC and Tempol, which suppress the ROS to which ATM responds [80,81,82], impact fatty liver disease.

In addition to developing longer lived animal models to study fatty liver disease progression, assessing the mechanisms driving fibrosis formation is an important aspect that warrants further evaluation. Since activated hepatic stellate cells are responsible for collagen production and deposition, elucidating the reasons for stellate cell activation and the fate of the cells following activation may provide insight into the central steps involved in disease progression and provide additional targets for therapy.

BIBLIOGRAPHY

1. Cohen JC, Horton JD, Hobbs HH (2011) Human fatty liver disease: old questions and new insights. Science 332: 1519-1523.

2. Marchesini G, Bugianesi E, Forlani G, Cerrelli F, Lenzi M, et al. (2003) Nonalcoholic fatty liver, steatohepatitis, and the metabolic syndrome. Hepatology 37: 917-923.

3. Starley BQ, Calcagno CJ, Harrison SA (2010) Nonalcoholic fatty liver disease and hepatocellular carcinoma: a weighty connection. Hepatology 51: 1820-1832.

4. Williams CD, Stengel J, Asike MI, Torres DM, Shaw J, et al. (2011) Prevalence of nonalcoholic fatty liver disease and nonalcoholic steatohepatitis among a largely middle-aged population utilizing ultrasound and liver biopsy: a prospective study. Gastroenterology 140: 124-131.

5. Hardwick RN, Fisher CD, Canet MJ, Lake AD, Cherrington NJ (2010) Diversity in antioxidant response enzymes in progressive stages of human nonalcoholic fatty liver disease. Drug metabolism and disposition: the biological fate of chemicals 38: 2293-2301.

6. Caldwell S, Park SH (2009) The epidemiology of hepatocellular cancer: from the perspectives of public health problem to tumor biology. Journal of gastroenterology 44 Suppl 19: 96-101.

7. Gomaa AI, Khan SA, Toledano MB, Waked I, Taylor-Robinson SD (2008) Hepatocellular carcinoma: epidemiology, risk factors and pathogenesis. World journal of gastroenterology : WJG 14: 4300-4308.

8. Mehta K, Van Thiel DH, Shah N, Mobarhan S (2002) Nonalcoholic fatty liver disease: pathogenesis and the role of antioxidants. Nutrition reviews 60: 289-293.

9. Ong J, Younossi ZM, Reddy V, Price LL, Gramlich T, et al. (2001) Cryptogenic cirrhosis and posttransplantation nonalcoholic fatty liver disease. Liver transplantation : official publication of the American Association for the Study of Liver Diseases and the International Liver Transplantation Society 7: 797-801.

10. Gao D, Wei C, Chen L, Huang J, Yang S, et al. (2004) Oxidative DNA damage and DNA repair enzyme expression are inversely related in murine models of fatty liver disease. American journal of physiology Gastrointestinal and liver physiology 287: G1070-1077.

11. Browning JD, Horton JD (2004) Molecular mediators of hepatic steatosis and liver injury. The Journal of clinical investigation 114: 147-152.

12. Feldstein AE, Gores GJ (2005) Apoptosis in alcoholic and nonalcoholic steatohepatitis. Frontiers in bioscience : a journal and virtual library 10: 3093-3099.

13. Barzilai A, Yamamoto K (2004) DNA damage responses to oxidative stress. DNA repair 3: 1109-1115.

14. Larter CZ, Chitturi S, Heydet D, Farrell GC (2010) A fresh look at NASH pathogenesis. Part 1: the metabolic movers. Journal of gastroenterology and hepatology 25: 672-690.

15. Nagata K, Suzuki H, Sakaguchi S (2007) Common pathogenic mechanism in development progression of liver injury caused by non-alcoholic or alcoholic steatohepatitis. The Journal of toxicological sciences 32: 453-468.

16. Xu Z, Chen L, Leung L, Yen TS, Lee C, et al. (2005) Liver-specific inactivation of the Nrf1 gene in adult mouse leads to nonalcoholic steatohepatitis and hepatic neoplasia. Proceedings of the National Academy of Sciences of the United States of America 102: 4120-4125.

17. Marra F, Gastaldelli A, Svegliati Baroni G, Tell G, Tiribelli C (2008) Molecular basis and mechanisms of progression of non-alcoholic steatohepatitis. Trends in molecular medicine 14: 72-81.

18. Kusminski CM, Shetty S, Orci L, Unger RH, Scherer PE (2009) Diabetes and apoptosis: lipotoxicity. Apoptosis : an international journal on programmed cell death 14: 1484-1495.

19. Cazanave SC, Elmi NA, Akazawa Y, Bronk SF, Mott JL, et al. (2010) CHOP and AP-1 cooperatively mediate PUMA expression during lipoapoptosis. American journal of physiology Gastrointestinal and liver physiology 299: G236-243.

20. Feldstein A, Gores GJ (2004) Steatohepatitis and apoptosis: therapeutic implications. The American journal of gastroenterology 99: 1718-1719.

21. Machado MV, Cortez-Pinto H (2011) Cell death and nonalcoholic steatohepatitis: where is ballooning relevant? Expert review of gastroenterology & hepatology 5: 213-222.

22. Noguchi Y, Young JD, Aleman JO, Hansen ME, Kelleher JK, et al. (2011) Tracking cellular metabolomics in lipoapoptosis- and steatosis-developing liver cells. Molecular bioSystems 7: 1409-1419.

23. Sunny NE, Parks EJ, Browning JD, Burgess SC (2011) Excessive Hepatic Mitochondrial TCA Cycle and Gluconeogenesis in Humans with Nonalcoholic Fatty Liver Disease. Cell metabolism 14: 804-810.

24. Tang D, Lotze MT, Kang R, Zeh HJ (2011) Apoptosis promotes early tumorigenesis. Oncogene 30: 1851-1854.

25. Cazanave SC, Mott JL, Elmi NA, Bronk SF, Werneburg NW, et al. (2009) JNK1-dependent PUMA expression contributes to hepatocyte lipoapoptosis. The Journal of biological chemistry 284: 26591-26602.

26. Labi V, Erlacher M, Krumschnabel G, Manzl C, Tzankov A, et al. (2010) Apoptosis of leukocytes triggered by acute DNA damage promotes lymphoma formation. Genes & development 24: 1602-1607.

27. Michalak EM, Villunger A, Adams JM, Strasser A (2008) In several cell types tumour suppressor p53 induces apoptosis largely via Puma but Noxa can contribute. Cell death and differentiation 15: 1019-1029.

28. Luedde T, Beraza N, Kotsikoris V, van Loo G, Nenci A, et al. (2007) Deletion of NEMO/IKKgamma in liver parenchymal cells causes steatohepatitis and hepatocellular carcinoma. Cancer cell 11: 119-132.

29. Forbes S, Vig P, Poulsom R, Thomas H, Alison M (2002) Hepatic stem cells. The Journal of pathology 197: 510-518.

30. Michalak EM, Vandenberg CJ, Delbridge AR, Wu L, Scott CL, et al. (2010) Apoptosis-promoted tumorigenesis: gamma-irradiation-induced thymic lymphomagenesis requires Puma-driven leukocyte death. Genes & development 24: 1608-1613.

31. Kim JJ, Tannock IF (2005) Repopulation of cancer cells during therapy: an important cause of treatment failure. Nature reviews Cancer 5: 516-525.

32. Michalak EM, Jansen ES, Happo L, Cragg MS, Tai L, et al. (2009) Puma and to a lesser extent Noxa are suppressors of Myc-induced lymphomagenesis. Cell death and differentiation 16: 684-696.

33. Qiu W, Carson-Walter EB, Kuan SF, Zhang L, Yu J (2009) PUMA suppresses intestinal tumorigenesis in mice. Cancer research 69: 4999-5006.

34. Nakanishi Y, Shiraha H, Nishina S, Tanaka S, Matsubara M, et al. (2011) Loss of runt-related transcription factor 3 expression leads hepatocellular carcinoma cells to escape apoptosis. BMC cancer 11: 3.

35. Matsuzaki K (2011) Smad phosphoisoform signals in acute and chronic liver injury: similarities and differences between epithelial and mesenchymal cells. Cell and tissue research.

36. Povero D, Busletta C, Novo E, di Bonzo LV, Cannito S, et al. (2010) Liver fibrosis: a dynamic and potentially reversible process. Histology and histopathology 25: 1075-1091.

37. Yasui K, Hashimoto E, Komorizono Y, Koike K, Arii S, et al. (2011) Characteristics of patients with nonalcoholic steatohepatitis who develop hepatocellular carcinoma. Clinical gastroenterology and hepatology : the official clinical practice journal of the American Gastroenterological Association 9: 428-433; quiz e450.

38. Lu S, Shen KC, Wang Y, Brooks SC, Wang YA (2005) Impaired hepatocyte survival and liver regeneration in Atm-deficient mice. Human molecular genetics 14: 3019-3025.

39. Lavin MF (2008) Ataxia-telangiectasia: from a rare disorder to a paradigm for cell signalling and cancer. Nature reviews Molecular cell biology 9: 759-769.

40. Zhang N, Chen P, Khanna KK, Scott S, Gatei M, et al. (1997) Isolation of full-length ATM cDNA and correction of the ataxia-telangiectasia cellular phenotype. Proceedings of the National Academy of Sciences of the United States of America 94: 8021-8026.

41. Ditch S, Paull TT (2011) The ATM protein kinase and cellular redox signaling: beyond the DNA damage response. Trends in biochemical sciences.

42. Guo Z, Kozlov S, Lavin MF, Person MD, Paull TT (2010) ATM activation by oxidative stress. Science 330: 517-521.

43. McKinnon PJ (2004) ATM and ataxia telangiectasia. EMBO reports 5: 772-776.

44. Bakker JL, de Winter JP (2012) A role for ATM in hereditary pancreatic cancer. Cancer discovery 2: 14-15.

45. Roberts NJ, Jiao Y, Yu J, Kopelovich L, Petersen GM, et al. (2012) ATM mutations in patients with hereditary pancreatic cancer. Cancer discovery 2: 41-46.

46. Shen L, Yin ZH, Wan Y, Zhang Y, Li K, et al. (2012) Association between ATM polymorphisms and cancer risk: a meta-analysis. Molecular biology reports 39: 5719-5725.

47. Bredemeyer AL, Sharma GG, Huang CY, Helmink BA, Walker LM, et al. (2006) ATM stabilizes DNA double-strand-break complexes during V(D)J recombination. Nature 442: 466-470.

48. Guo Z, Deshpande R, Paull TT (2010) ATM activation in the presence of oxidative stress. Cell cycle 9: 4805-4811.

49. Bakkenist CJ, Kastan MB (2003) DNA damage activates ATM through intermolecular autophosphorylation and dimer dissociation. Nature 421: 499-506.

50. So S, Davis AJ, Chen DJ (2009) Autophosphorylation at serine 1981 stabilizes ATM at DNA damage sites. The Journal of cell biology 187: 977-990.

51. Barlow C, Brown KD, Deng CX, Tagle DA, Wynshaw-Boris A (1997) Atm selectively regulates distinct p53-dependent cell-cycle checkpoint and apoptotic pathways. Nature genetics 17: 453-456.

52. Matsuoka S, Rotman G, Ogawa A, Shiloh Y, Tamai K, et al. (2000) Ataxia telangiectasia-mutated phosphorylates Chk2 in vivo and in vitro. Proceedings of the National Academy of Sciences of the United States of America 97: 10389-10394.

53. Bartkova J, Rezaei N, Liontos M, Karakaidos P, Kletsas D, et al. (2006) Oncogene-induced senescence is part of the tumorigenesis barrier imposed by DNA damage checkpoints. Nature 444: 633-637.

54. Matsuoka S, Ballif BA, Smogorzewska A, McDonald ER, 3rd, Hurov KE, et al. (2007) ATM and ATR substrate analysis reveals extensive protein networks responsive to DNA damage. Science 316: 1160-1166.

55. Armata HL, Golebiowski D, Jung DY, Ko HJ, Kim JK, et al. (2010) Requirement of the ATM/p53 tumor suppressor pathway for glucose homeostasis. Molecular and cellular biology 30: 5787-5794.

56. Zha S, Sekiguchi J, Brush JW, Bassing CH, Alt FW (2008) Complementary functions of ATM and H2AX in development and suppression of genomic instability. Proceedings of the National Academy of Sciences of the United States of America 105: 9302-9306.

57. Li M, Fang X, Baker DJ, Guo L, Gao X, et al. (2010) The ATM-p53 pathway suppresses aneuploidy-induced tumorigenesis. Proceedings of the National Academy of Sciences of the United States of America 107: 14188-14193.

58. Elson A, Wang Y, Daugherty CJ, Morton CC, Zhou F, et al. (1996) Pleiotropic defects in ataxia-telangiectasia protein-deficient mice. Proceedings of the National Academy of Sciences of the United States of America 93: 13084-13089.

59. Rogers AB, Boutin SR, Whary MT, Sundina N, Ge Z, et al. (2004) Progression of chronic hepatitis and preneoplasia in Helicobacter hepaticus-infected A/JCr mice. Toxicologic pathology 32: 668-677.

60. Maurer KJ, Rao VP, Ge Z, Rogers AB, Oura TJ, et al. (2007) T-cell function is critical for murine cholesterol gallstone formation. Gastroenterology 133: 1304-1315.

61. Sobreira C, Davidson M, King MP, Miranda AF (1996) Dihydrorhodamine 123 identifies impaired mitochondrial respiratory chain function in cultured cells harboring mitochondrial DNA mutations. The journal of histochemistry and cytochemistry : official journal of the Histochemistry Society 44: 571-579.

62. Harlow E, Lane D (2006) Lysing Tissue-Culture Cells for Immunoprecipitation. Cold Spring Harbor Protocols 2006: pdb.prot4531.

63. Matsuzawa N, Takamura T, Kurita S, Misu H, Ota T, et al. (2007) Lipid-induced oxidative stress causes steatohepatitis in mice fed an atherogenic diet. Hepatology 46: 1392-1403.

64. Barzilai A, Rotman G, Shiloh Y (2002) ATM deficiency and oxidative stress: a new dimension of defective response to DNA damage. DNA repair 1: 3-25.

65. Barlow C, Hirotsune S, Paylor R, Liyanage M, Eckhaus M, et al. (1996) Atm-deficient mice: a paradigm of ataxia telangiectasia. Cell 86: 159-171.

66. Xu Y, Ashley T, Brainerd EE, Bronson RT, Meyn MS, et al. (1996) Targeted disruption of ATM leads to growth retardation, chromosomal fragmentation during meiosis, immune defects, and thymic lymphoma. Genes & development 10: 2411-2422.

67. Kinner A, Wu W, Staudt C, Iliakis G (2008) Gamma-H2AX in recognition and signaling of DNA double-strand breaks in the context of chromatin. Nucleic acids research 36: 5678-5694.

68. McKinnon PJ (2011) ATM and the Molecular Pathogenesis of Ataxia Telangiectasia. Annual review of pathology.

69. Yu J, Zhang L (2008) PUMA, a potent killer with or without p53. Oncogene 27 Suppl 1: S71-83.

70. Krizhanovsky V, Yon M, Dickins RA, Hearn S, Simon J, et al. (2008) Senescence of activated stellate cells limits liver fibrosis. Cell 134: 657-667.

71. Zhan SS, Jiang JX, Wu J, Halsted C, Friedman SL, et al. (2006) Phagocytosis of apoptotic bodies by hepatic stellate cells induces NADPH oxidase and is associated with liver fibrosis in vivo. Hepatology 43: 435-443.

72. Canbay A, Friedman S, Gores GJ (2004) Apoptosis: the nexus of liver injury and fibrosis. Hepatology 39: 273-278.

73. Villunger A, Michalak EM, Coultas L, Mullauer F, Bock G, et al. (2003) p53- and drug-induced apoptotic responses mediated by BH3-only proteins puma and noxa. Science 302: 1036-1038.

74. Farinati F, Cardin R, Bortolami M, Grottola A, Manno M, et al. (2002) Estrogens receptors and oxidative damage in the liver. Molecular and cellular endocrinology 193: 85-88.

75. Nunomura A, Perry G, Pappolla MA, Wade R, Hirai K, et al. (1999) RNA oxidation is a prominent feature of vulnerable neurons in Alzheimer's disease. The Journal of neuroscience : the official journal of the Society for Neuroscience 19: 1959-1964.

76. Woodbine L, Brunton H, Goodarzi AA, Shibata A, Jeggo PA (2011) Endogenously induced DNA double strand breaks arise in heterochromatic DNA regions and require ataxia telangiectasia mutated and Artemis for their repair. Nucleic acids research 39: 6986-6997.

77. El-Serag HB (2011) Hepatocellular carcinoma. The New England journal of medicine 365: 1118-1127.

78. Dowman JK, Armstrong MJ, Tomlinson JW, Newsome PN (2011) Current therapeutic strategies in non-alcoholic fatty liver disease. Diabetes, obesity & metabolism 13: 692-702.

79. Foster T, Budoff MJ, Saab S, Ahmadi N, Gordon C, et al. (2011) Atorvastatin and antioxidants for the treatment of nonalcoholic fatty liver disease: the St Francis Heart Study randomized clinical trial. The American journal of gastroenterology 106: 71-77.

80. Reliene R, Schiestl RH (2007) Antioxidants suppress lymphoma and increase longevity in Atm-deficient mice. The Journal of nutrition 137: 229S-232S.

81. Reliene R, Schiestl RH (2008) Experimental antioxidant therapy in ataxia telangiectasia. Clinical medicine Oncology 2: 431-436.

82. Schubert R, Erker L, Barlow C, Yakushiji H, Larson D, et al. (2004) Cancer chemoprevention by the antioxidant tempol in Atm-deficient mice. Human molecular genetics 13: 1793-1802.